

BALL ON PLATE BALANCING SYSTEM

by

Greg Andrews, RPI
Chris Colasuonno, RPI
Aaron Herrmann, RPI

ECSE-4962 Control Systems Design
Final Project Report
April 28, 2004

Rensselaer Polytechnic Institute

Abstract

The problem of controlling an open-loop unstable system presents many unique and interesting challenges. A specific example of an open-loop unstable system is the ball-on-plate system, a two-dimensional extension of the ball-and-beam problem. Among the interesting challenges of such a system is the indirect control of the ball using the angles of the plate. In this paper, a complete physical system and controller design is explored from conception to modelling to testing and completion.

Contents

1	Introduction	1
2	Professional and Societal Consideration	4
3	Design Procedure	6
3.1	Model development	6
3.2	Control development	8
3.3	Physical design	9
3.4	Touch screen subsystem development	10
4	Design Details	13
4.1	Modeling	13
4.2	Control	14
4.3	Simulation	17
4.4	Touch screen subsystem	20
5	Design Verification	25
6	Costs	29
7	Conclusions	31
A	Diagrams and Figures	33
B	Datasheets	44
C	MATLAB Code	47
D	CAD Drawings	53
E	Team contributions	57
F	Team resumes	58

List of Figures

1.1	Project Design Plan	3
3.1	Ball on Beam Free Body Diagram	8
3.2	Touch screen A/D conversion layout	11
4.1	Observer State Estimation - Plate	16
4.2	Observer Error - Plate	16
4.3	Simulink Block Diagram	18
4.4	Plate Sinusoid Tracking - Closeup	19
4.5	Ball Position Sinusoid Tracking - 1 rad/sec	19
4.6	Simulink touch screen interface	21
4.7	Simulink touch screen packet conversion	21
4.8	Touch screen filter - Bode plot	22
4.9	Touch screen output filtering	23
4.10	Touch screen output filtering (close-up)	23
5.1	Model validation - drop	26
5.2	Step response - 0.5 radians	26
5.3	Sine wave tracking - 2 radians/sec	27
A.1	Pan Axis Friction Data	33
A.2	Tilt Axis Friction Data	34
A.3	Frequency Response - Pan Axis	34
A.4	Frequency Response - Tilt Axis	35
A.5	Observer State Estimation - Ball	35
A.6	Observer Error - Ball	36
A.7	Frequency Response - Outer-loop	36
A.8	Plate Sinusoid Tracking - 3 rad/sec	37
A.9	Ball Position Step Response	37
A.10	Ball Circular Trajectory	38
A.11	Nonlinear plate dynamics block diagram	39
A.12	Linear ball dynamics block diagram	39
A.13	Gravity compensation block diagram	40
A.14	Friction compensation block diagram	40
A.15	VR Sink Parameters Window	41

A.16 Virtual Reality Simulation Block Diagram	41
A.17 Virtual Reality Animation Window	42
A.18 Gravity cancellation	42
A.19 Touch screen output test (Simple)	43
A.20 Touch screen output test (Complex)	43
D.1 Full System	53
D.2 Body A Coordinate Definitions	54
D.3 Body B Coordinate Definitions	54
D.4 Axle	55
D.5 Encoder Side Bracket	55
D.6 Motor Side Bracket	56
D.7 Yoke Base	56

List of Tables

3.1	Touch screen pin-out	10
4.1	Gain and Phase Margins	17
4.2	Touch screen controller packet composition	20
6.1	List of parts	29
6.2	List of raw materials	29
6.3	Labor costs	30

Chapter 1

Introduction

The goal of this project is to develop a ball-on-plate balancing system, capable of controlling the position of a ball on a plate for both static positions and smooth paths. We intend that the initially horizontal plate will be tilted along each of two horizontal axes in order to control the position of the ball. Each tilting axis will be operated on by an electric motor. Each motor will be controlled using software, with a minimum of position feedback for control. The position of the ball on the plate will be sensed through a resistive touch screen.

The ball-on-plate system as implemented has limited consumer appeal. The challenge of balancing, however, is a problem under continuous study for applications from robotics to transportation, often extensions of the inverted pendulum project. Therefore, the system can present many challenges and opportunities as an educational tool to university students studying control systems engineering.

The initial objective of the project is to maintain a static ball position on the plate, rejecting position disturbances. An extension of this objective is movement to specified positions on the system: given a position, a trajectory is plotted and the ball is moved to the new location. If this is extended further, trajectories such as a circle or a figure-eight can be followed given judicious choices for ball position requests.

Characterizing system specs for such a system is difficult, notably because the desired motion is for an piece of the system that is *indirectly* controlled. The controller cannot directly manipulate the ball, and therefore deciding on the specs of the plate controller, in terms of rise time, settling time, and steady-state error is difficult. With this in mind, the specifications of the overall system are $< 2\%$ error in the position of the ball, with a settling time of less than 2 seconds, and for a nominal rotational speed (of the plate) of 1.35 rad/sec. This, in turn, mandates excellent response from the plate controller, including quick rise times, rapid settling, and negligible steady-state error. Any error in the plate controller gets compounded into the ball position, so overshoot, steady-state error and slow settling all present obstacles to ideal performance in the ball positioning.

The project design plan is shown in Figure 1.1. As shown, the project needs to be broken into three sub-projects: the sensor system, the physical system, and the controller. These three projects will be developed independently by the team, and then integrated into a complete system. The sensor subsystem consists of the circuitry and software that generate coordinates from the touch screen. The physical system refers to

the design and machining of parts needed to construct the large yoke and axle, as well as the new motor bracket, which are necessary to bear the weight of the touch screen. The control system includes not only the modelling and simulation of the system as a whole, but additionally, the design of the controllers: one for the ball position and another for the plate angles.

One of the major obstacles to integration and implementation is the reading of position coordinates from the touch. A RS-232 serial card is supplied with the touch screen, however, the average position report rate is 80-100 positions/second. Another obstacle is the system itself, which is open-loop unstable: the design must take into account not only the dynamics of the two axis plate system, but also the dynamics of the heavy steel ball moving around on the surface of the system.

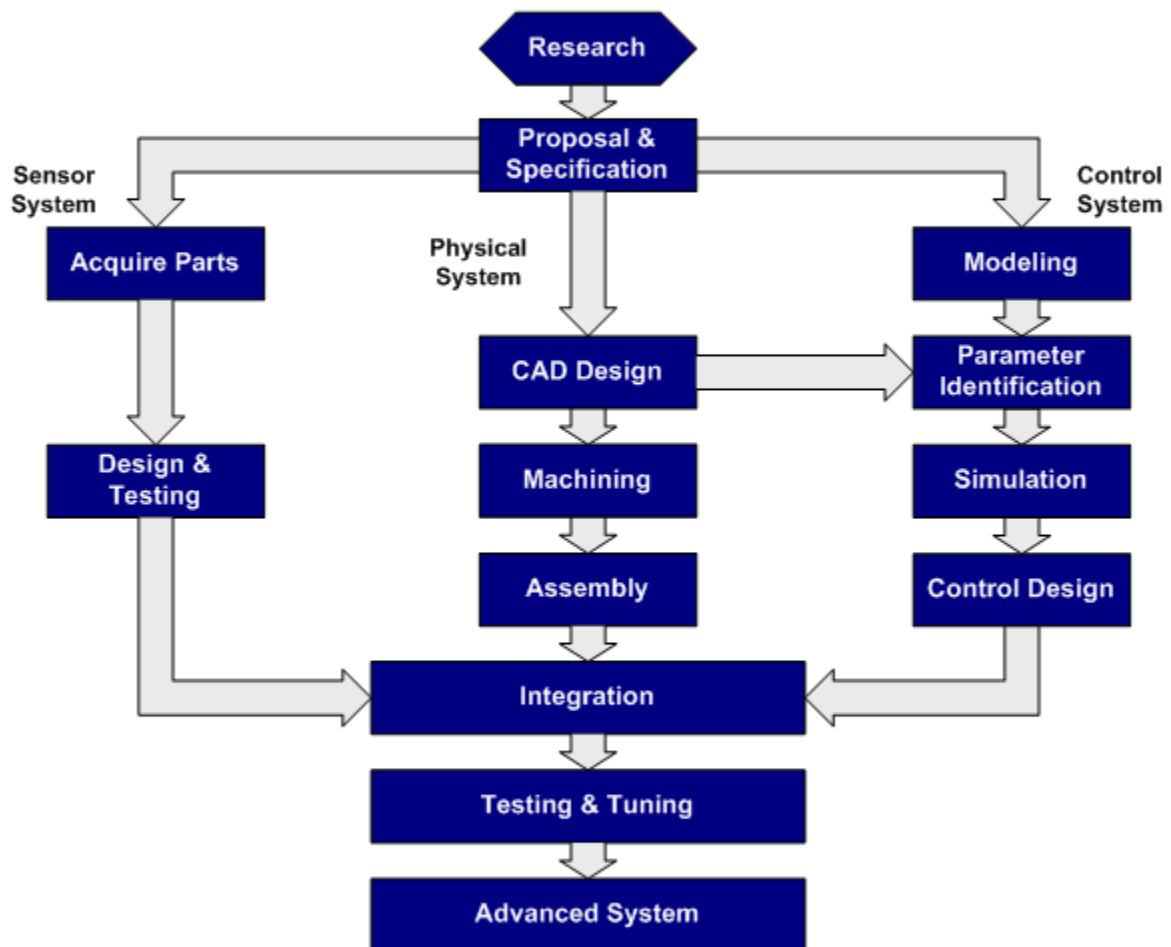


Figure 1.1: Project Design Plan

Chapter 2

Professional and Societal Consideration

As a product, the ball-on-plate system presents little in the way of a commercially viable product, except perhaps as an exercise in control systems education. In that pursuit, however, there are still several prior projects that tread the same path as this system, and thus patent protection would be difficult. Of immediate similarity is the project created by the Professor Kevin Craig at Rensselaer Polytechnic Institute in the Mechatronics program [4]. Ultimately, the differences between the project developed by Professor Craig's team and the project described in this report are implementational, with the ultimate objective of balancing being the same. Professor Craig's project however is inherently stable by design, whereas the project described herein is naturally astable, therefore making the control somewhat more difficult. A second project of similar scope was found upon search, created by Professors Graham Goodwin, Stefan Graebe and Mario Salgado [5] from the University of Newcastle, Australia. The mechanism for balancing here is the same, however, the feedback for ball position is generated using image processing techniques and a CCD camera placed above the system. While investigating other projects, and additional search was made for patents protecting designs or technology related to this system. This, however, yielded no systems related or similar in operation to this project in the listings of protected inventions and designs.

If the project's applications are taken to be academic and educational, considerations must still be made with regard to the system's safety and durability. Design decisions were therefore made that emphasized the goal of a safe product that could be used for educational purposes. Wherever possible, metal edges were filed and screw heads countersunk to prevent injury during a possible system instability. A polycarbonate plate was placed across the rotational axis to protect the glass substrate of the touch screen, and to protect the user should the touch pad become damaged. The glass in the touch screen is also chemically treated (i.e. tempered), and while much stronger than untreated glass, also has the unique characteristic that instead of forming sharp shards under fracture, it creates small, harmless bits of glass. With regard to software, torque thresholds could be added to prevent violent behavior under unstable conditions. Another safety measure is inherent to the operation of the touch screen coordinate system - should the ball break contact with the plate, the system returns (0,0) positions. Should the ball leave the plate entirely, the system will simply stay put. If desired, a further level of safety could even shut the system down upon retrieval of 0s to

the coordinate generator. Further development should also look into a more secure mounting system, since simple metal C-clamps can loosen under repeated stress.

Should the system head into further revision, in preparation for manufacturing, several changes would have to be made to make the system both commercially viable and capable of mass manufacture. Primary concern rests on the inherent fallibility of the touch screen. Other touch sensitive technologies exist, albeit more expensive, however it might be possible to source a supplier capable of building a resistive touch screen that uses a polycarbonate or plastic substrate. This would cause a negligible change in cost, amortized over a large production run, and would be a major boon to the overall product safety. Wire shielding is also of major concern: the power wires running into the motors present a large, fluctuating electric field, which tends to wreak havoc with the encoder wires, because the last 15 cm of wire are unshielded. This would be a simple change resulting in a significantly better behaved system. Additionally, it might be recommended to replace the secondary motor with a smaller, lighter unit, albeit with less torque. The secondary axis is a light and balanced load, and requires significantly lower torques. This would in turn reduce the load on the primary motor by reducing rotating mass, improving efficiency as well as safety.

Chapter 3

Design Procedure

3.1 Model development

In order to design a control system that will accurately control the position of the ball, a highly accurate model of the entire system's dynamics must be developed. As the accuracy of the model increases, the uncertainty to be dealt with by the control effort will decrease. The model for our plate dynamics comes from the general equation of motion for a multibody system,

$$M(\theta)\ddot{\theta} + B(\dot{\theta}) + C(\theta, \dot{\theta})\dot{\theta} + G(\theta) = \tau \quad (3.1)$$

where M is the mass-inertia matrix of the system, B is the friction term, C is the velocity coupling matrix, and G is the gravity loading vector. In most pan/tilt applications, there is no gravity loading on the first joint. However, due to the altered orientation of our system (See Figure D.1), we have gravity loading terms for both joints, as can be seen in Equation 3.2, the gravity loading vector for our system. Numeric values for these terms can be found in Section 4.1.

$$G(\theta) = \begin{bmatrix} -m_a g \sin(\theta_1) l_{ca1} - m_a g \cos(\theta_1) l_{ca2} - m_b g \sin(\theta_1) \cos(\theta_2) l_{cb1} - m_b g \cos(\theta_1) l_{cb2} - m_b g \sin(\theta_1) \sin(\theta_2) l_{cb3} \\ -m_b g \cos(\theta_1) \sin(\theta_2) l_{cb1} + m_b g \cos(\theta_1) \cos(\theta_2) l_{cb3} \end{bmatrix} \quad (3.2)$$

Unfortunately, using the linear control theory that we have learned thus far, it becomes difficult to develop a control system for our fully nonlinear model. Because of this, the system must be linearized about a trim condition in which the state derivatives are zero, i.e. $(\dot{\theta}, \theta) = (0, \theta_d)$. This operating point should be specified in the angular region in which the system will spend the majority of its time, in our case $\theta_d = 0$. The linearization of the system can be derived as follows: The mass-inertia matrix can simply be evaluated at $\theta = \theta_d$. Due to the trigonometric nonlinear terms in the gravity loading vector, we use a Taylor Series expansion, keeping only the linear terms, and use the small angle assumption: $\sin(\theta) \approx \theta$ and $\cos(\theta) \approx 1$. Since G is a function of both angles, $f(\theta_1, \theta_2)$, we evaluate the gradient of G to determine the derivative terms of the Taylor Series expansion with respect to both variables. The velocity coupling matrix C drops out completely since all terms involve a θ^2 term. The friction term, B , is separated into its viscous and coulomb

components, and the coulomb terms are treated as an input disturbance. The result of this linearization is:

$$M(\theta_d)\ddot{\theta} + \frac{\partial G(\theta_d)}{\partial \theta}(\theta - \theta_d) + F_v\dot{\theta} = Bu - F_c \text{sgn}(\dot{\theta}) \quad (3.3)$$

where Bu represents the control torque.

In order to facilitate the state-feedback control law $u = -\mathbf{K}x$ (See Section 3.2), we must form the state-space realization for this dynamic system. Defining our state vector as:

$$x := \begin{bmatrix} \theta_1 & \theta_2 & \dot{\theta}_1 & \dot{\theta}_2 \end{bmatrix}^T \quad (3.4)$$

we can solve for our state variables:

$$\begin{aligned} x_1 &= \theta - \theta_d \\ x_2 &= \dot{\theta} \\ \dot{x}_1 &= x_2 \\ \dot{x}_2 &= M^{-1}(\theta_d) \left[Bu - F_c \text{sgn}(\dot{\theta}) - F_v x_2 - \frac{\partial G(\theta_d)}{\partial \theta} x_1 \right] \end{aligned} \quad (3.5)$$

treating Bu as the control input, and $F_c \text{sgn}(\dot{\theta})$ as an input disturbance, the state-space form becomes:

$$\begin{aligned} \dot{x} &= \begin{bmatrix} 0 & 0 & 1 & 0 \\ 0 & 0 & 0 & 1 \\ \underbrace{-M^{-1}(\theta_d) \frac{\partial G}{\partial \theta}}_{2 \times 2} & \underbrace{-M^{-1} F_v}_{2 \times 2} \end{bmatrix} x + \begin{bmatrix} 0 & 0 \\ M^{-1}(\theta_d) & 0 \\ 0 & M^{-1}(\theta_d) \end{bmatrix} u \\ y &= \begin{bmatrix} 1 & 0 & 0 & 0 \\ 0 & 1 & 0 & 0 \end{bmatrix} x \end{aligned} \quad (3.6)$$

With this linearized system, we can design a control law that will control the plate's angular position based on torque input. In addition to the plate dynamics, the ball's response to plate position must be considered. For our purposes, it should suffice to treat the ball and plate system as two decoupled ball on beam systems. In addition, we will ignore any rolling friction that may occur between the ball and plate. This greatly simplifies the model, and makes for easier control design. From the free body diagram in Figure 3.1, we can obtain the dynamic equations that govern the ball's motion [3]:

$$\begin{aligned} 0 &= \left(\frac{J}{r^2} + m \right) \ddot{x} + mg \sin(\theta) \\ \ddot{x} &= -\frac{mg \sin(\theta)}{\left(\frac{J}{r^2} + m \right)} \\ \ddot{x} &= -\frac{mg}{\left(\frac{J}{r^2} + m \right)} \theta \end{aligned} \quad (3.7)$$

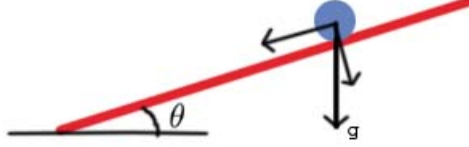


Figure 3.1: Ball on Beam Free Body Diagram

Using the small angle approximation $\sin(\theta) \approx \theta$, we obtain Equation 3.7, where J is the ball's inertia, r is the ball's radius, m is the ball's mass, and g is the gravitational constant. Extended to two dimensions, the state-space realization of the system becomes:

$$\begin{bmatrix} \dot{x} \\ \dot{y} \\ \ddot{x} \\ \ddot{y} \end{bmatrix} = \begin{bmatrix} 0 & 0 & 1 & 0 \\ 0 & 0 & 0 & 1 \\ 0 & 0 & 0 & 0 \\ 0 & 0 & 0 & 0 \end{bmatrix} \begin{bmatrix} x \\ y \\ \dot{x} \\ \dot{y} \end{bmatrix} + \begin{bmatrix} 0 & 0 \\ 0 & 0 \\ -\frac{mg}{(\frac{J}{r^2} + m)} & 0 \\ 0 & -\frac{mg}{(\frac{J}{r^2} + m)} \end{bmatrix} \theta \quad (3.8)$$

With these linearized equations of motion for the plate and ball, we can begin to design our controller.

3.2 Control development

To control the Ball on Plate Balancing System, we have decided to employ a full state-feedback controller. Though classical control design approaches may have been sufficient, we felt as though we would achieve better results with state-feedback. One reason that state-feedback control is particularly advantageous is that all information regarding oscillatory modes and initial conditions is available, which is not the case with classical frequency domain methodologies [6]. The state-feedback control will also utilize an observer to estimate the velocity states of the system. This will be mentioned in more detail later in this section.

Before developing the controller and observer, we must first check to see that the system is both controllable and observable, i.e. we can influence all system states through our control input, and that they will be visible at the output. To verify this, we must ensure that the Controllability and Observability matrices are full rank:

$$C = [B \quad AB \quad A^2B \quad \dots \quad A^{n-1}B]$$

$$O = [C \quad CA \quad CA^2 \quad \dots \quad CA^{n-1}]^T$$

For our linearized systems as given in Equations 3.6 and 3.8, they are both fully controllable and observable, so we may continue on to the control design phase.

For plate control, we use a Linear Quadratic Regulator (LQR). This serves to find the optimal control input, $u(t)$ that will drive the system from its initial states, $x(t_0)$ to some final value, $x(t_f)$, while minimizing a (quadratic) cost function:

$$J = \int_0^{t_f} \mathbf{x}^T \mathbf{Q} \mathbf{x} + \mathbf{u}^T \mathbf{R} \mathbf{u} dt \quad (3.9)$$

where \mathbf{Q} is the state penalty matrix, and \mathbf{R} is the control penalty matrix [7]. These are user defined matrices, whose proper selection will achieve the desired time-domain response. The optimal feedback gain matrix, \mathbf{K} can be found using $\mathbf{K} = \mathbf{R}^{-1}\mathbf{B}^T\mathbf{P}$ where \mathbf{P} is a positive definite solution to the Steady State Riccati Equation:

$$\mathbf{PBR}^{-1}\mathbf{B}^T\mathbf{P} = \mathbf{PA} + \mathbf{A}^T\mathbf{P} + \mathbf{Q} \quad (3.10)$$

Once the feedback gain matrix has been found, we can form the control law

$$u = -\mathbf{K}x \quad (3.11)$$

that will drive our the system states to the desired values. This, however, assumes that we can measure all four of the states as defined in the state vector in Equation 3.4. In reality, we can only directly measure x_1 and x_2 , the angular position of the plate, and not the velocity. For this reason, we develop a state observer that will estimate the values of x_3 and x_4 . This is done by creating a copy of the linear dynamic equations, and adding an output term:

$$\begin{aligned} \dot{\hat{x}} &= \mathbf{A}\hat{x}(k) + \mathbf{B}u(k) + \mathbf{L}(y(k) - \hat{y}(k)) \\ \hat{y}(k) &= \mathbf{C}\hat{x}(k) \end{aligned} \quad (3.12)$$

where \hat{x} is the observer's estimate of the system states, u is the system input, y is the plant output, and \hat{y} is the observer output. The \mathbf{L} matrix ensures that the observer error, $\hat{x}(k) - x(k)$ converges to zero [2]. Much like LQR was used to determine the optimal feedback gain matrix, \mathbf{K} , we will use a Kalman filter to determine the optimal observer gain matrix, \mathbf{L} . Normally, a Kalman filter bases its calculation on the covariance matrices of the process and measurement noise. However, for simplification, we will use a more heuristic approach, much like deciding the values for the \mathbf{Q} and \mathbf{R} matrices for the LQR control. More detail on this can be found in Section 4.2. Once the observer gain matrix has been found, we can easily implement the control in (discrete) state-space form:

$$\begin{aligned} \hat{x}(k+1) &= (\mathbf{A} - \mathbf{BK} - \mathbf{LC})\hat{x}(k) + \mathbf{L}y(k) \\ u(k) &= -\mathbf{K}\hat{x}(k) \end{aligned} \quad (3.13)$$

where the output of the observer becomes $u(k)$, the control torque, and the output of the plant, i.e. encoder feedback, is the input to the observer.

The same procedure is followed to develop a controller for the ball dynamics. However, instead of using LQR to determine the feedback gain matrix, \mathbf{K} , we simply use pole placement, the mathematics of which we will forego discussing in detail in this report. See [8] for a discussion of pole placement, as well as a more detailed discussion of state-feedback control and LQR in general. LQR is used to determine the observer gains. Details on this can be found in Section 4.2.

3.3 Physical design

Several physical components in addition to the motors, shafts, gears, belts, and encoders were necessary in order to realize the construction of the system. These custom made parts included a specialized axle, yoke, and motor mounting bracket. Each of these parts of the system were machined out of aluminum stock and their full dimensions are included in Appendix D. Specific attributes of the system of course required the parts to have certain features. The lengths and widths of the yoke were designed to fit the size and shape of

the touch screen that was used in the project with some slight clearance along the long side of the yoke to allow for wiring to move freely.

The special axle was designed to support the touch screen on the tilt axis. It was formed of several pieces to allow for set screw adjustment of the height. This allowed for materials of varying thickness to be placed on the axle while keeping the actual plane of the touch screen coincident with the axes of rotation. In the final design these materials included a polycarbonate plate, the touch screen itself, and a rubber membrane to provide friction that will force the ball to roll instead of slide.

Finally the motor mount bracket was created to fix the tilt axis motor to the system. It was designed to place the motor directly behind the yoke to reduce the inertia effects of the heavy motor as much as possible.

3.4 Touch screen subsystem development

Ball position feedback is accomplished through the usage of an analog resistive touch screen element. Screens of this type are often used in public information kiosks and cashier stations, allowing the user to interact with the screen directly. As the feedback in this system, the touch screen will read the application of pressure by a steel ball and track it as it moves within the active portion of the screen.

An analog resistive touch screen works using a simple design. Two layers of material are coated with indium tin oxide (ITO) to give them a known resistance, something between 100 and 500 $\Omega/sq.$ depending on the manufacturer and the application. The two layers are then placed 90° offset from each other on top of a glass or polycarbonate substrate, with a grid of transparent insulating dots separating the layers. Silver bus bars are placed at the edges to allow the application of voltage across the layers. To generate a touch position, the user or an object must exceed the activation force of the screen, pressing the two layers together. This creates an electrical connection between the layers. However, both X and Y axes cannot be read simultaneously, because the concept works by applying a voltage across one layer, and looking for the voltage that appears on the other layer. Therefore, the system works by alternately applying a voltage to one layer and reading off of the other. The voltages are then read in by an analog-to-digital (A/D) converter to be used as a coordinate value[1].

There are, however, several types of analog resistive touch screens, notably 4-wire, 5-wire and 8-wire. These designations refer to the number of wires between the screen and the screen controller. 4-wire screens operate by applying voltage across the two wires for one layer, and reading a voltage from the ground wire of the other layer. The voltage application and read operation then swaps around for the other layer. The 5-wire screens use the bottom layer for both axes measurements, applying voltage across the top layer only. This simplifies measurement and voltage application duties over the 4-wire screen. The 8-wire screen is an extension of the 4-wire screen, using the additional 2-wires per layer to provide a stable voltage gradient. This makes the 8-wire screen immune to voltage and resistance fluctuations due to ambient heat and humidity or aging of the screen. The pin configuration for an 8-wire screen is shown in Table 3.1[1].

Table 3.1: Touch screen pin-out

Axis	Xe^+	Xe^-	Ye^+	Ye^-	Xs^+	Xs^-	Ys^+	Ys^-
X	5v	GND	NC	READ	Ref+	Ref-	NC	NC
Y	NC	READ	5v	GND	NC	NC	Ref+	Ref-

Due to pricing and immediate availability, an 8-wire screen was selected for this project. The advantages of the 8-wire over the 4-wire screen aren't really relevant to this project, however the stability of the 8-wire screen certainly helps during testing. The difficulty with the 8-wire screen, however, is the requirement for ratiometric A/D converters. Ratiometric A/D converters use the applied voltage at the location being converted as the reference for the conversion, instead of using a static reference. This accounts for variations in the supply voltage, as well as variations in the transmission lines caused by noise or interference. Originally, it was planned that the A/D conversion for the touch screen would be done by the ARCS system, using full 16-bit resolution and a 1 ms sampling period. The ARCS board A/D converters are unfortunately not ratiometric. Further complicating things was a significant difficulty in generating position coordinates using a regulated power supply and an oscilloscope. The choice was therefore made to use the RS-232 touch screen controller included with touch screen purchase. Using 10-bits of resolution enables the controller to have a maximum theoretical 1024x1024 positions on the surface of the touch screen. This, however, is limited to a subset of the full range, (100-900)x(100-900) positions, due to losses in drive voltage from the various transmission lines leading to the screen itself. The layout of the voltage ranges with the corresponding digital values is shown in Figure 3.2[1].

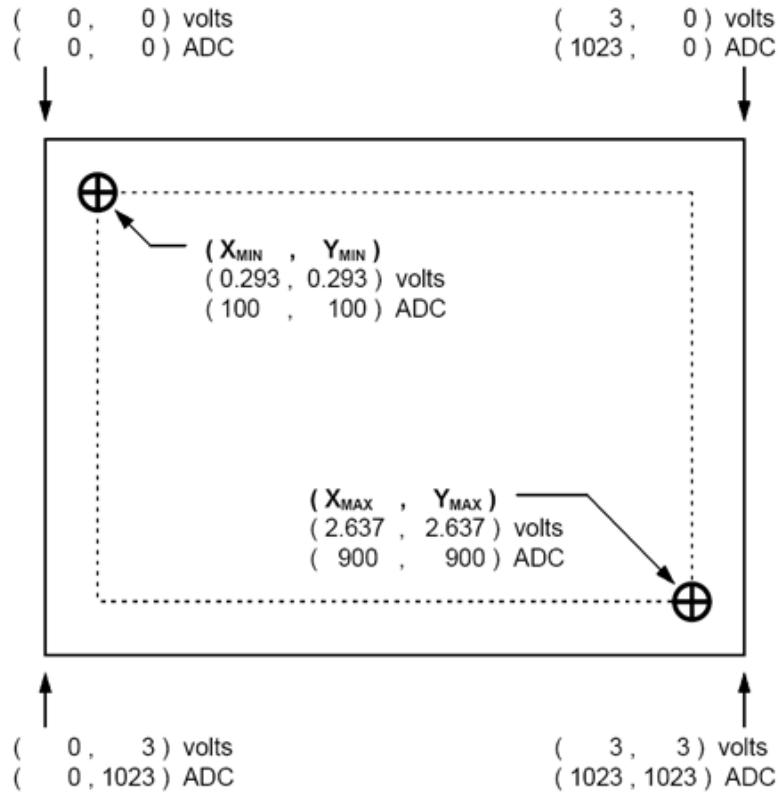


Figure 3.2: Touch screen A/D conversion layout

Using the serial touch screen controller with MATLAB and xPC Target requires using the RS-232 blocks available in the xPC Target Simulink block library. During regular operation, the controller sends data

regardless of any receiving device. Therefore, MATLAB merely has to process the data as it comes in, convert the digital values to real-world coordinates, and then pass them along to the ball controller. This is discussed further in Section 4.4.

The analog resistive touch screen was chosen as the ball feedback for this project for several reasons. The primary reason is simplicity, both of the sensing operation and the circuitry/software required to generate coordinates. This is even further enhanced by the availability of simple serial controller cards and chips which can generate position coordinates without any configuration or setup. Certainly, if one were so inclined, a video processing system could be constructed that is capable of generating similar results. However, a system of this type of equal ability to the touch screen is limited by a number of things:

1. A CCD capable of generating frame rates fast enough to match what a simple touch screen controller is capable of would be prohibitively expensive (≥ 100 frames/sec)
2. The video from the CCD needs to be handed off to a frame-grabber capable of reading video at the same frame rate (≥ 100 frames/sec) which is prohibitively expensive
3. MATLAB xPC Target is very limited in the ways in which it can receive data, as it doesn't really have a vast driver set, and therefore any frame grabber card would need a custom driver in order to pass video frames to MATLAB
4. Once the video is brought into MATLAB, further processing still needs to be done to process the image and find the centroid of the ball
5. The position coordinate processing algorithm would need to be sufficiently robust to deal with varying brightness and reflections and noise in the video signal

This list isn't to suggest that a video processing system isn't possible with a ball-on-plate system, merely that with the resources available for this college design course, a touch screen made the most sense.

Other touch sensitive technologies exist outside of the basic analog resistive system. These include infrared, capacitive, near field imaging (NFI), and surface acoustic wave (SAW). Each has advantages that make it better for certain applications. However, in trying to track a ball, capacitive sensing requires the electrical activity of a human hand. Infrared is also not as accurate as the other technologies and is sensitive to variations in ambient light. Of those technologies remaining, NFI, SAW and resistive, resistive touch screens are by far the least expensive to acquire and implement, and are very durable. This made the resistive touch screen the ideal choice for this application, due to budget constraints.

Chapter 4

Design Details

4.1 Modeling

To determine numerical values for the state-space representation of the system dynamics as derived in Section 3.1, we must first identify the unknown parameters of the system, i.e. inertia and friction. To identify the inertia of the system, a Solidworks model of the system was made. The inertia of each link about its center of mass with respect to our defined coordinate systems (as shown in Figures D.2 and D.3) was determined by Solidworks. The values for the inertia tensors are shown in Equation 4.1. It should be noted that the inertia tensor of link B, J_b , only contains diagonal values, whereas J_a does not. This is due to the fact that Body B has uniform mass, and Body A does not due to the offset mounting of the motor as seen in Figure D.1

$$J_a = \begin{bmatrix} .0277 & -.0001 & -.0003 \\ -.0001 & .0209 & .0065 \\ -.0003 & .0065 & .0070 \end{bmatrix} \quad J_b = \begin{bmatrix} .0045 & 0 & 0 \\ 0 & .0010 & 0 \\ 0 & 0 & .0035 \end{bmatrix} \quad (4.1)$$

Identification of the friction in the system was performed as follows: A Simulink model capable of measuring the encoder and outputting constant voltages was used in conjunction with a MATLAB script to repeatedly estimate the velocity of each joint. For each of 200 voltage increments from minus two volts to plus two volts, the motor was allowed to turn for ten seconds so that it would reach steady state velocity. The last four seconds were then averaged to obtain a single value for steady state velocity for that particular torque (voltage). In addition, a one second ten volt spike was added in the beginning of each run in order to overcome the stiction of the system. By plotting this data and finding a least squares approximation for the data, the coulomb and viscous friction were found as the intercept and slope of the regression line, respectively. The plots for each axis are shown in Figures A.1 and A.2.

With these parameters identified, we can substitute numerical values into Equation 3.6 and begin to design our controller. However, since we have fully identified the system model, we can use feedback linearization to, in effect, cancel out the gravity and viscous friction terms. This will be discussed further in Section 4.2.

Assuming that gravity and friction can be perfectly cancelled, we can obtain the linear state-space model either from Equation 3.6, or using MATLAB's `linmod()` function. The resulting state-space is shown in Equation 4.2.

$$\dot{x} = \begin{bmatrix} 0 & 0 & 1 & 0 \\ 0 & 0 & 0 & 1 \\ 0 & 0 & 0 & 0 \\ 0 & 0 & 0 & 0 \end{bmatrix} x + \begin{bmatrix} 0 & 0 \\ 0 & 0 \\ 66.73 & 0 \\ 0 & 100.8037 \end{bmatrix} u \quad (4.2)$$

Equation 4.2 shows the linear dynamic equations that are used to develop the control system.

For the ball dynamics, all values in Equation 3.8 are known constants. The inertia of the ball, J , can be found from the equation for the inertia of a sphere [9]:

$$J = \frac{2}{5}mr^2$$

Substituting in the following values:

$$\begin{aligned} m &= .13kg \\ g &= 9.81m/sec^2 \\ r &= .0158m \end{aligned} \quad (4.3)$$

we obtain the final state-space representation of the ball dynamics, as shown in Equation 4.4.

$$\begin{bmatrix} \dot{x} \\ \dot{y} \\ \ddot{x} \\ \ddot{y} \end{bmatrix} = \begin{bmatrix} 0 & 0 & 1 & 0 \\ 0 & 0 & 0 & 1 \\ 0 & 0 & 0 & 0 \\ 0 & 0 & 0 & 0 \end{bmatrix} \begin{bmatrix} x \\ y \\ \dot{x} \\ \dot{y} \end{bmatrix} + \begin{bmatrix} 0 & 0 \\ 0 & 0 \\ -7 & 0 \\ 0 & -7 \end{bmatrix} \theta \quad (4.4)$$

4.2 Control

The control scheme for the Ball on Plate Balancing System consists of two loops: an inner loop to control the motor torque based on a desired plate angle, and an outer loop to command a plate angle based on a desired ball location. In order to successfully implement this design, the inner loop must have a much faster response than the outer loop. Since the inner loop can only be designed to be as fast as physical limitations allow (motor torque, etc.), we must intentionally design the outer loop to be slower.

As mentioned in Section 3.2, we decided upon the use of a Linear Quadratic Regulator for the purposes of plate positioning. Successful implementation of this depends on our defined state and control penalty matrices, \mathbf{Q} and \mathbf{R} . Since we want to accurately track the angular position of the ball, and care less about the angular velocity, we choose the \mathbf{Q} matrix to have a high weighting on the position states. Adjustment of the \mathbf{R} matrix will either promote or penalize the control effort. By altering these values, we can further adjust the time-domain response, while making sure not to operate in the saturation region of our motors. For this reason, it is important to take the motor saturation into account when designing the simulation.

The final values of \mathbf{Q} and \mathbf{R} are shown in Equation 4.5.

$$\mathbf{Q} = \begin{bmatrix} 1000 & 0 & 0 & 0 \\ 0 & 1000 & 0 & 0 \\ 0 & 0 & 1 & 0 \\ 0 & 0 & 0 & 1 \end{bmatrix} \quad \mathbf{R} = \begin{bmatrix} .5 & 0 \\ 0 & .5 \end{bmatrix} \quad (4.5)$$

With these state penalty matrices, the state gain matrix was calculated with MATLAB, and is shown in Equation 4.6.

$$\mathbf{K} = \begin{bmatrix} 44.7214 & 0 & 1.8277 & .0001 \\ 0 & 44.7214 & .0001 & 1.6992 \end{bmatrix} \quad (4.6)$$

This places the closed loop eigenvalues at:

$$(\mathbf{A} - \mathbf{BK}) = [-88.0, -138.8, -33.8, -32.5]^T \quad (4.7)$$

When designing an observer to estimate the system states, it is important to make the observer's dynamics much faster than that of the closed-loop system. As mentioned in Section 3.2, we used a Kalman filter to calculate the optimal observer gain matrix, \mathbf{L} . Just as with the LQR design for the controller, the \mathbf{Q} and \mathbf{R} matrices we chosen to give the best results. The optimal solution would be derived using the process and sensor noise covariances, however we simply use the matrices as "weights" as we did with LQR. The final values for these matrices are seen in Equation 4.8.

$$\mathbf{Q} = \begin{bmatrix} 100000 & 0 \\ 0 & 100000 \end{bmatrix} \quad \mathbf{R} = \begin{bmatrix} .01 & 0 \\ 0 & .01 \end{bmatrix} \quad (4.8)$$

resulting in the observer gain matrix:

$$\mathbf{L} = \begin{bmatrix} 205.4 & -.0438 \\ -.0438 & 252.5 \\ 21101 & -10.03 \\ -10.03 & 31876 \end{bmatrix} \quad (4.9)$$

which places the system's closed-loop eigenvalues at:

$$(\mathbf{A} - \mathbf{BK} - \mathbf{LC}) = [-211 \pm j186, -163 \pm j149]^T \quad (4.10)$$

Normally, the observer eigenvalues should be roughly 5-10 times faster than the closed-loop eigenvalues. In our case, they are not quite that fast, however the observer estimates the system states very well, and increasing the speed of the observer's dynamics yields negligible differences. Figure 4.1 shows how well the observer tracks the system states for a step response, and Figure 4.2 shows the observer error as a function of time. It should be noted that these responses were generated using the nonlinear plate dynamics.

Bode plots showing the open-loop frequency response of the inner-loop are shown in Figures A.3 and A.4. Gain and phase margins for both the inner-loop and outer-loop are summarized in Table 4.1.

A similar design procedure is used to develop the outer-loop controller for the ball dynamics in Equation 4.4. Instead of LQR, we use pole placement to move the closed-loop eigenvalues to the desired locations. For our case, we chose to place all closed-loop poles at $s = -1.25 \pm j1.5$. This corresponds to a natural frequency of

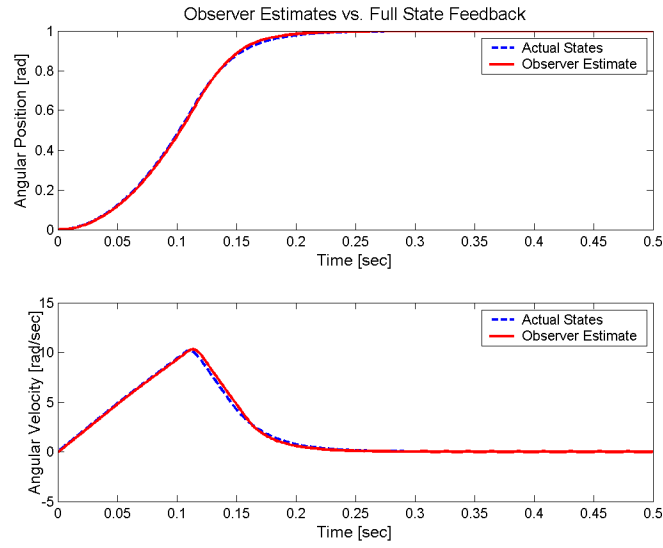


Figure 4.1: Observer State Estimation - Plate

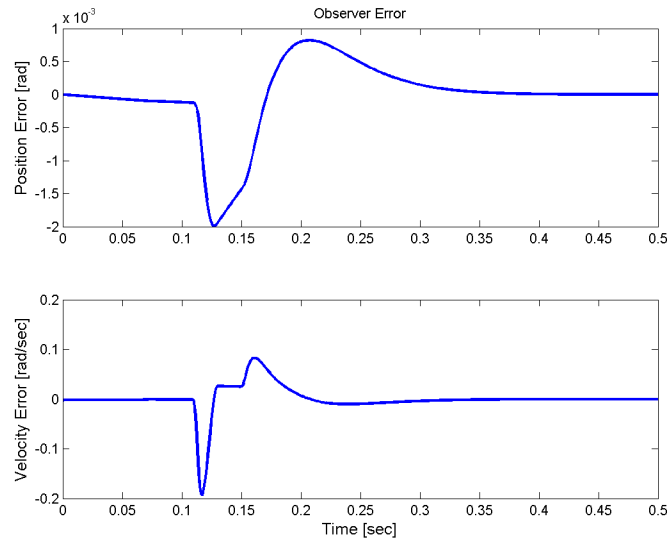


Figure 4.2: Observer Error - Plate

$w_n = 1.95$ and a damping ratio of $\zeta = .64$. Using MATLAB's `place()` command, we compute the feedback gain matrix to be:

$$\mathbf{K} = \begin{bmatrix} -.5446 & 0 & -.3571 & 0 \\ 0 & -.5446 & 0 & -.3571 \end{bmatrix} \quad (4.11)$$

After several design iterations, we find the \mathbf{Q} and \mathbf{R} matrices to be:

$$\mathbf{Q} = \begin{bmatrix} 100000 & 0 & 0 & 0 \\ 0 & 100000 & 0 & 0 \\ 0 & 0 & 1 & 0 \\ 0 & 0 & 0 & 1 \end{bmatrix} \quad \mathbf{R} = \begin{bmatrix} .01 & 0 \\ 0 & .01 \end{bmatrix} \quad (4.12)$$

resulting in the observer gain matrix:

$$\mathbf{L} = \begin{bmatrix} 3162.3 & 0 \\ 0 & 3162.3 \\ 10 & 0 \\ 0 & 10 \end{bmatrix} \quad (4.13)$$

The open-loop frequency response for the outer-loop is shown in Figure A.7.

Table 4.1: Gain and Phase Margins

	Gain	Phase
Pan	∞	-147 deg at 38.4 rad/sec
Tilt	-187 dB at 0 rad/sec	-147 deg at 47.2 rad/sec
Ball	70 dB at 112 rad/sec	76.1 deg at 0.974 rad/sec

Figure A.5 shows how well the observer tracks the system states, and Figure A.6 shows the observer error as a function of time. It can be seen in the figures that the observer is able to estimate the system states with almost no error. Note that the vertical scale in both Figures 4.2 and A.6 is on the order of 10^{-3} .

4.3 Simulation

When any engineering problem is approached, it is desirable, if not absolutely necessary that a simulation of the system is made. This allows the engineer to analyze and test their design before actual implementation. The need for this becomes obvious if one considers very large, expensive systems such as an aircraft. One would obviously not want to build an aircraft, and then fly it to see if the flight controls work. It is important to remember that the validity of a simulation depends greatly on the accuracy of the model. For this reason, we developed a simulation around the full nonlinear model of our Ball on Plate system. The simulation takes into account nonlinearities such as gravity loading, coulomb and viscous friction, torque saturation, encoder quantization, touch screen quantization, and the multiple sampling rates of our system. Figure 4.3 shows a Simulink block diagram that represents the entire Ball on Plate Balancing System. This section will discuss the function and purpose of each block. The trajectory generation block serves command the desired ball position. This may take on the form of a specific coordinate, or some path such as a sinusoid. The control/observer blocks are the state-space implementations of the state-feedback controller, $u = -\mathbf{K}x$, and

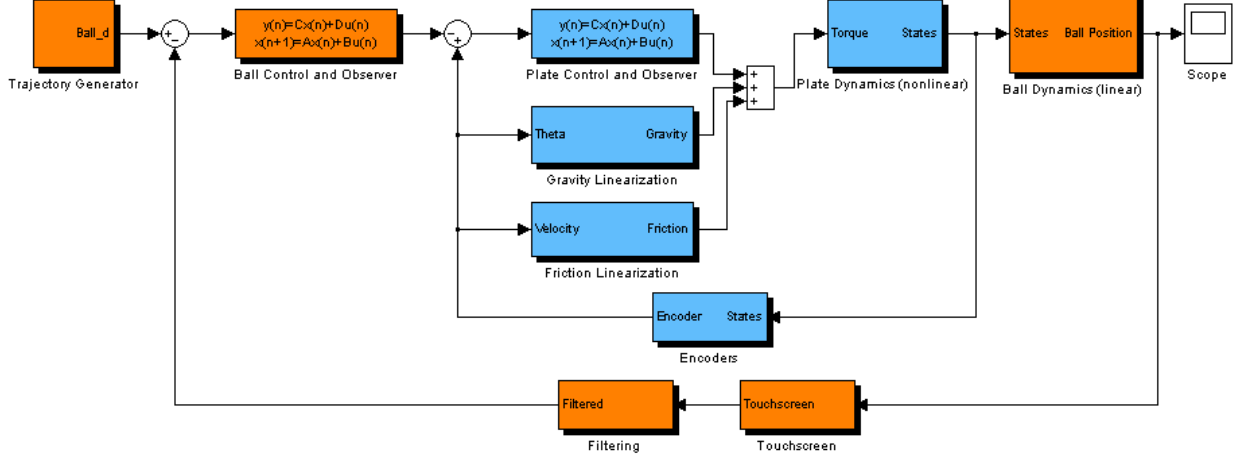


Figure 4.3: Simulink Block Diagram

the observer estimate, \hat{x} . The gravity and friction linearization blocks simulate the feedback linearization that we are employing to negate the nonlinear gravity and friction terms of the system. They are then added to the control torque (output from the plate controller), and passed onto the nonlinear plate dynamics block. This block is the heart of the simulation, and takes into account all of the aforementioned nonlinearities. In the actual implementation, this block is replaced by the amplifier block. The output of this block (plate angle) is fed into the linear ball dynamics block. In reality, this block would be replaced by the encoders. The output of the ball dynamics is fed into a touch screen simulation. This block takes into account the quantization and sampling rate of the touch screen. The interpolation filter, as described in Section 4.4, is also included in the simulation.

Various plate and ball control tests were run with the simulation before the actual control implementation. The first test was the tracking ability of plate control (a step response can be seen back in Figure 4.1). Figures A.8 and 4.4 show the results for tracking a sinusoid at 3 rad/sec. The closeup shows the slight error at low velocity. This error becomes magnified in the actual implementation due to friction. The next simulations were a step response and sinusoid tracking for the ball position. Figures A.9 and 4.5 show the results of this. The sinusoid tracking shows a very large phase delay. This stems from the fact that the outer-loop must be slow to allow the plate to position itself properly. Unfortunately, this speed difference causes a large phase delay. However, despite the delay, the ball tracks the amplitude of the sinusoid very well. Both responses were for a desired amplitude of 0.05 m, which is roughly half the distance of the plate, and 1 rad/sec. Additionally, a circular ball trajectory was commanded. The results of this are shown in Figure A.10.

To better visualize the simulation results, a 3D animation was generated using MATLAB's Virtual Reality Toolbox. Here, we will briefly describe the steps taken to create this animation. The reader is encouraged to refer to the Virtual Reality Toolbox documentation for more detailed information. The first step in creating the animation was to export the Solidworks model as a VRML97 file. Solidworks exports a single *.vrmf file, which contains a model for each part as defined in Solidworks. Using the V-Realm Builder by Ligos Corp. (included with the virtual reality toolbox), we can group specific parts to form the bodies, as defined

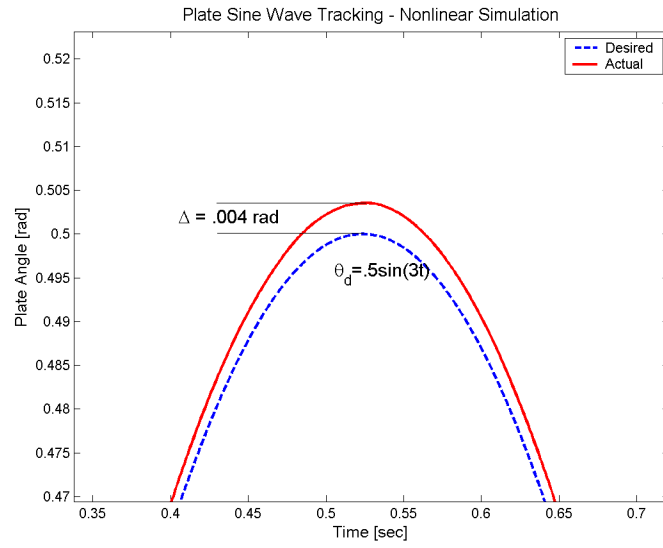


Figure 4.4: Plate Sinusoid Tracking - Closeup

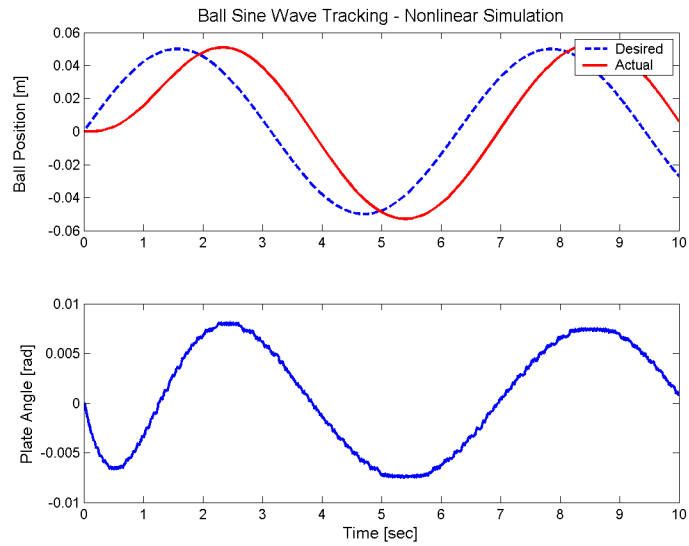


Figure 4.5: Ball Position Sinusoid Tracking - 1 rad/sec

in Figures D.2 and D.3. A group for Body B was created as a sub-group within Body A, and the ball was placed in a sub-group within Body B. Then, in each of these groups, the rotational axes were defined. These are the axes which the virtual reality toolbox will use to control the movement of the objects. Using this new VRML97 file, we can create a Simulink block diagram to control the animation. A VR Sink block is placed in the Simulink diagram, and the *.vrmf file we created previously is loaded into this file. In the VRML tree pane in the properties of the VR Sink block, we enable the checkboxes that correspond to the rotational axes that we defined using V-Realm Builder. Rotation nodes were selected for the two main bodies, and a translation node was used for the ball. Figure A.15 shows the block parameters window for the VR Sink block. The "view" button in the block parameters window initializes the animation, and shows the object. Finally, data from a previously run simulation, which is stored to the workspace, is fed into the VR Sink block, as shown in Figure A.16. Once the Simulink simulation is run, the animation begins. This animation is able to replicate any results from the simulation. Figure A.17 shows the output window.

4.4 Touch screen subsystem

The touch screen interface to MATLAB relies entirely on the capabilities of the 3M Dynapro SC3 serial interface controller for its operation. Every touch controller "report" consists of an X-Y coordinate pair. The SC3 controller takes these X-Y coordinate pairs it generates and converts them into sets of three 8-bit packets which can be converted into coordinate pairs. The actual coordinate values are 10-bit values, that are actually spread across the three separate packets as shown in Table 4.2. Note that in the table, the P bit refers to the status of the 'pen', or the object touching the pad: 1 is pen down, 0 is pen up. Also note that x9 refers to the 10th bit of the 10-bit x coordinate number, and so forth for all x_k and $y_k[1]$.

Table 4.2: Touch screen controller packet composition

Packet/Bit #	7	6	5	4	3	2	1	0
#1 (<i>sync</i>)	1	P	x_9	x_8	x_7	y_9	y_8	y_7
#2 (<i>data</i>)	0	x_6	x_5	x_4	x_3	x_2	x_1	x_0
#3 (<i>data</i>)	0	y_6	y_5	y_4	y_3	y_2	y_1	y_0

All of these packets are sent asynchronously and without prompting: as soon as the touch screen receives sufficient pressure for the controller to register a touch, the system begins to send data. In order to process this data, and get the resultant coordinate information into the real-time computer, a serial interface needs to be created in MATLAB Simulink that can be compiled for the xPC Target system.

The basic overall system utilizes the binary receive block in Simulink to retrieve data as sets of three 1-byte packets as described in the manual. The RS232 Setup block sets the link parameters as 2400 bps, and 8-N-1 - 8 bits per packet, no parity, and 1 stop bit. Normally, Simulink is unable to utilize binary numbers, however, the Communications Toolbox allows conversion to and from binary. This makes possible the individual bit manipulation necessary to move the 8-bit packets from the controller into the 10-bit binary words that the controller's A/D converter creates. The Simulink diagrams for this system can be seen in Figures 4.6 and 4.7.

After assembling the Simulink system and using the steel ball to generate coordinate paths, it becomes obvious that while the touch screen does generate a great many points, it generates a number of coordinates

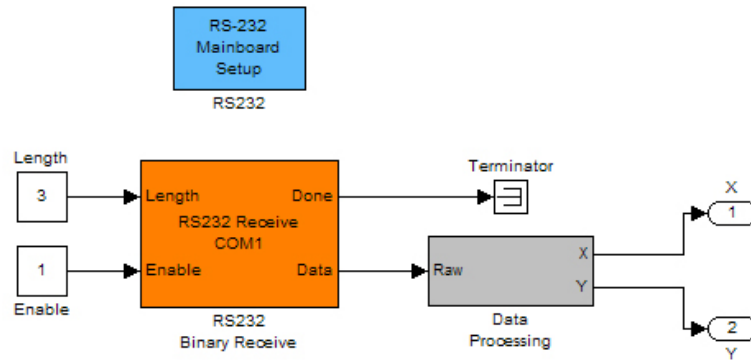


Figure 4.6: Simulink touch screen interface

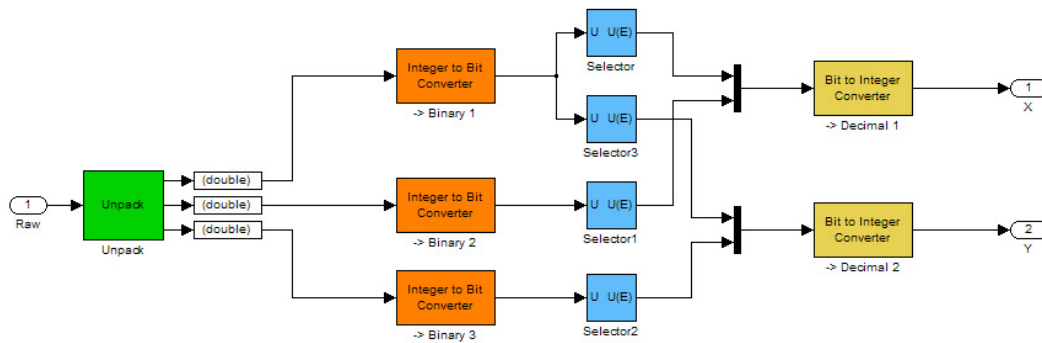


Figure 4.7: Simulink touch screen packet conversion

in the same area due to settling time settings in the controller. The result is the series of steps shown in Figure 4.9. If integrated with the ball controller and the plate controller, this stepping would result in very abrupt movement and poor performance.

After several unsuccessful attempts to send the controller configuration commands, it was decided that the easiest alternative was to pass the generated coordinates through a low-pass filter. The abrupt changes in the output coordinates are equivalent to a step command, so in order to smooth it, a simple first order low-pass filter was created, with a cutoff at 50 radian/second. This cutoff was chosen to maximize data retention, namely small fluctuations in output, but to remove the large jumps in output that would cause problems with the controllers. The transfer function, in continuous time, is

$$F_c = \frac{1}{1 + \frac{s}{50}} \quad (4.14)$$

If this is converted to discrete time, using the controller's sampling period of 1 ms with a zero-order hold, the transfer function is

$$F_d = \frac{0.04877}{z - 0.9512} \quad (4.15)$$

The bode plot of this filter is shown in Figure 4.8. The -3db point of the now discrete filter is around 50 radians/sec as designed, with a decent roll-off, though that isn't terribly important. The objective is to reduce the amplitude of much higher frequencies, which this filter does as shown in Figure 4.9, looking at the now much smoother sine wave.

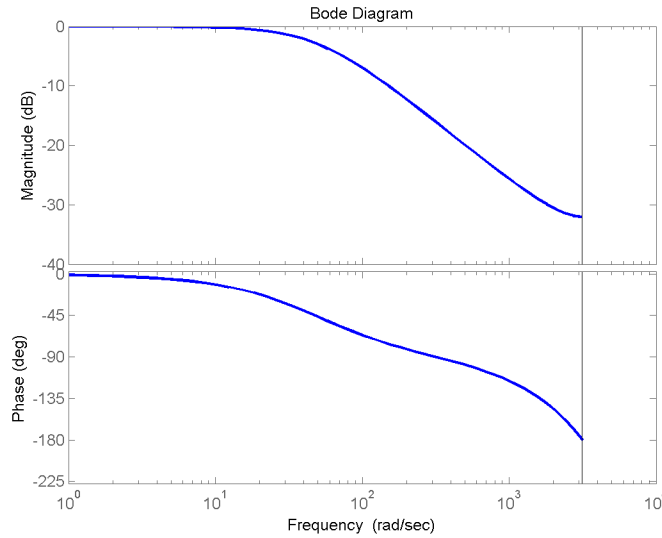


Figure 4.8: Touch screen filter - Bode plot

With the coordinates smoothed, the remaining work is to scale and map the coordinates. First of all, the coordinates generated by the touch screen are based on a reference point of (0,0) in the top left corner, as seen in Figure 3.2. The controller, however, assumes (0,0) to be the center of touch screen, which is really

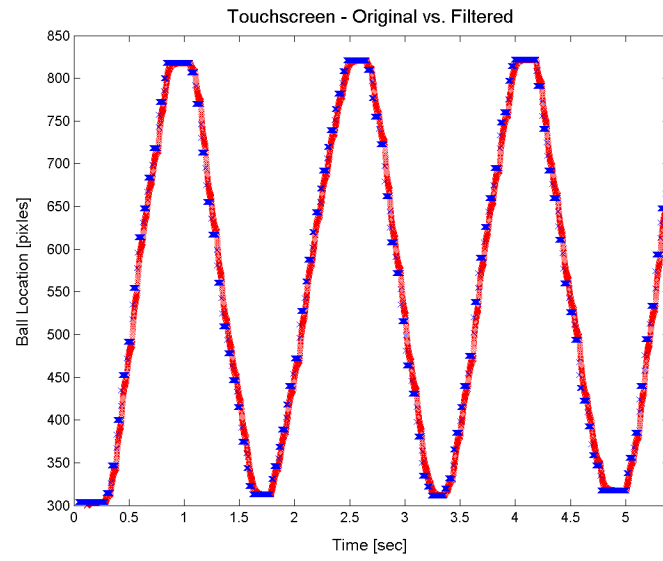


Figure 4.9: Touch screen output filtering

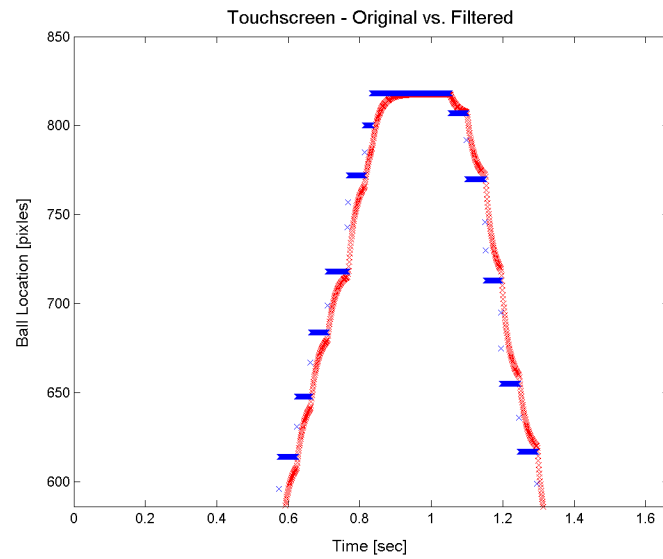


Figure 4.10: Touch screen output filtering (close-up)

coordinate point (512,512). To map the coordinates to this new space, each generated coordinate is reduced by 512 to find the new coordinate. The controller is also expecting displacements from the center (0,0) point in meters. To scale the coordinates to meters, the known resolution and size of the touch screen is utilized to find the meters per digital level generated by the touch screen controller.

$$\frac{.12065 \text{ } m}{512 \text{ } levels} = 2.356 \times 10^4 meters/level \text{ } (X)$$

$$\frac{.09525 \text{ } m}{512 \text{ } levels} = 1.860 \times 10^4 meters/level \text{ } (Y)$$

Chapter 5

Design Verification

Several steps were taken to verify the design of both the individual components of the ball on plate system, as well as the system as a whole. These included comparison of simulated and experimental results of: the effects on the inactive system due to a sudden release from an unstable point, step responses, sine wave tracking, and a friction and gravity cancellation experiment. The touch screen design was also verified through several experiments, and finally the overall performance of the system was rigorously tested as the controller was tuned for the best results. Videos are available upon request and included with the electronic version of this report.

In the first experiment, the system was set up with the motors disabled but the encoders active. The system was then rotated by hand and raised up to the level position at which the system will operate. Dropping the system and allowing gravity to do its work, the response on the pan axis was recorded by the encoder. This same scenario was then developed in simulation, and the plots of position versus time for each were compared.

Shown in Figure 5.1 are the resulting plots for both the actual and simulated responses. The graph demonstrates that there is a close match including the rise times, settling times, and shape of the response.

A step response for a 0.5 rad position command and then a 2 rad/sec sine wave input were also applied to the system both in the actual physical system. The plots for each are shown in Figures 5.2 and 5.3.

By examining the plots, the step responses of the simulated and experimental form a close match. In addition, sine wave tracking matches nearly perfectly. With the exception of a slight flattening at the top of the experimental resulting sine wave, the desired, simulated, and experimental are all identical.

In order to further verify the design, a friction and gravity cancellation experiment was devised. By inputting only the friction and gravity terms that are used for feedback linearization in the system, it was possible to observe the effects of the cancellation on the physical system. When the experiment was running, the once heavy and unbalanced physical system could be moved to any position by hand with ease and this position was held in place. In addition, a light push on the system resulted in the system spinning about the pan axis six to eight times due to the reduced friction. Figure A.18 shows a plot of the exactly constant torque output for the system at its balancing position is shown. The torque output value was 0.38 N-m. This value matched both simulation as well as hand-written calculations for the amount of torque necessary to hold

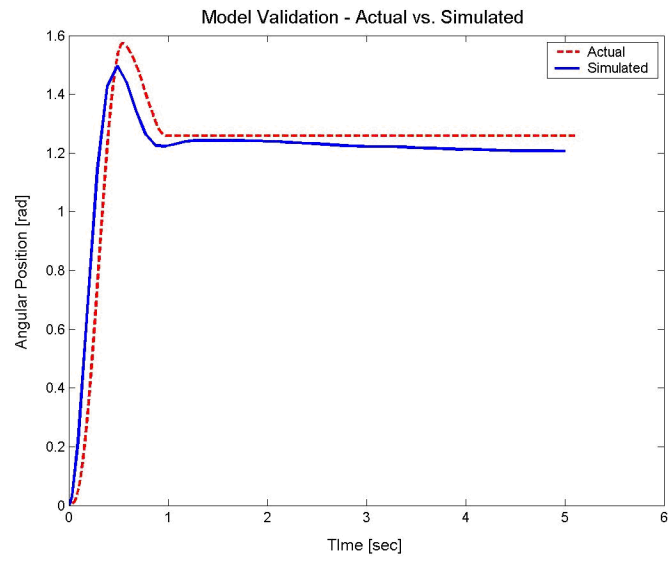


Figure 5.1: Model validation - drop

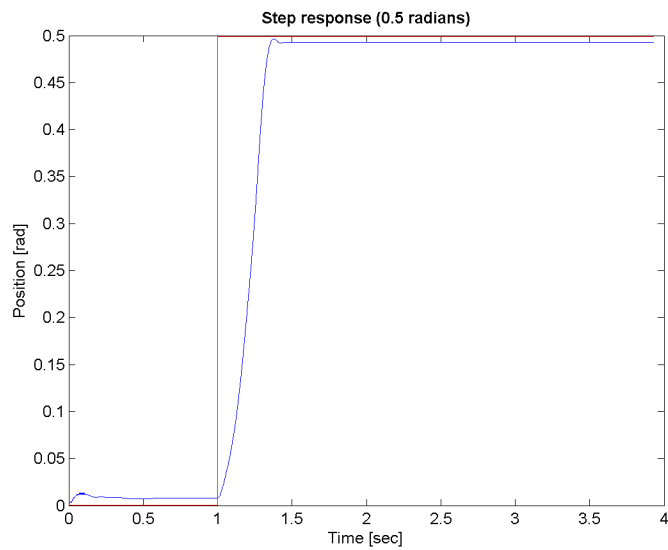


Figure 5.2: Step response - 0.5 radians

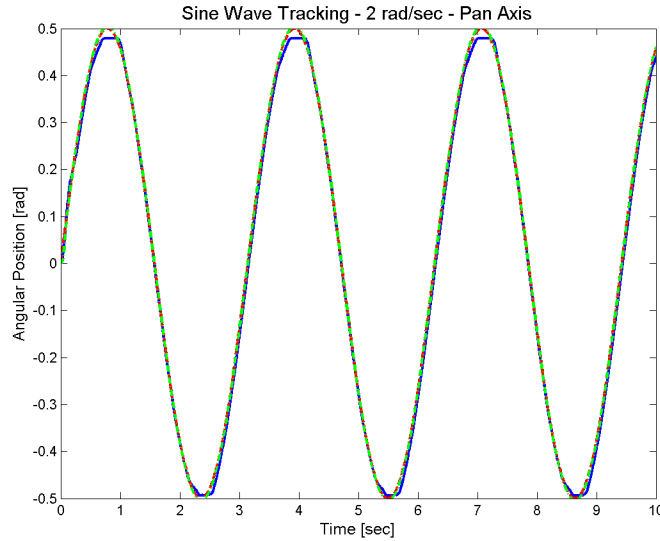


Figure 5.3: Sine wave tracking - 2 radians/sec

up the heavy system. A video demonstration is available upon request and included with the multimedia version of this report.

As discussed earlier, the touch screen interface was designed through and xPC Target serial interface to the touch screen controller card. Upon completion of the design various tests were performed to view the subsystems ability with tracking the ball. Figures A.19 and A.20 are plots of several inputs traced on the touch screen by actually rolling the ball. The first is simply a square with diagonals drawn across it. The second is a more complicated rendition of the name "Chris" in cursive handwriting. Both showed very good results.

Final design verification of course occurred during the testing and tuning of the final system. Through rigorous testing, sometimes complicated by touch screen malfunction, the various objectives of the project for static balancing and path following by the ball were observed. After some tuning, ball balancing for a static position worked well. Given a commanded location of the origin (center of the plate), the system was capable of correcting even extreme disturbances to the ball location within a minimal amount of time and oscillations about the desired point. Steady state error was also at a minimum. In addition, path following along a straight line worked well to a degree, though there was some oscillation about the line as the ball rolled along its path. For a circle trajectory, the best result for the balls path was more of an oval shape. Demonstration videos qualitatively well demonstrate the results of the design, however touch screen failure immediately following these good results has prevented any collection of quantitative verification data such as desired versus actual ball position information for static positions. This is unfortunate; however it is extremely fortunate that such excellent video was captured before the failure of the touch screen. Upon replacement, further data could be collected.

A simple tolerance analysis test to verify the gain and phase margins (qualitatively) is to give the system a

disturbance while in operation. While the system was being commanded to follow a sine wave input, we held the yoke from moving by hand. After letting go, the system sped up to catch up with the desired trajectory, and then fell back into sync.

Chapter 6

Costs

Table 6.1: List of parts

Item	Qty	Cost	Total	Source
1 1/4" diam. 440C stainless ball	1	\$9.17	\$9.17	McMaster-Carr
3M Dynapro 95640 10.4" 8-wire resistive touch screen	1	\$39.00	\$39.00	Ebay
3M Dynapro SC3 4/8-wire resistive touch screen controller	1			Ebay
Pittman motor GM9234S017 (pan)	1	\$97.59	\$97.59	Supplied
Pittman motor GM9234S017 (tilt)	1	\$97.59	\$97.59	Supplied
Pan gear A	1	\$9.97	\$9.97	Supplied
Pan gear B	1	\$22.02	\$22.02	Supplied
Tilt gear A	1	\$7.95	\$7.95	Supplied
Tilt gear B	1	\$22.02	\$22.02	Supplied
Pan belt	1	\$3.92	\$3.92	Supplied
Tilt belt	1	\$3.55	\$3.55	www.sdp-si.com
Misc screws		\$5.00	\$5.00	Home Depot
Total			\$269.61	

Table 6.2: List of raw materials

Item	Qty	Cost	Total	Source
1/2" aluminum stock	5 lb	\$4/lb	\$20.00	RPI Machine Shop
1/16" latex rubber membrane	1	\$9.38 - 12"x12"	\$9.38	McMaster-Carr
.093" Lexan panel	1	\$5.00 - 8"x10"	\$5.00	Home Depot
Total			\$34.38	

Table 6.3: Labor costs

Description	Hours	Cost	Total
Andrews, Greg [Engineer]	300	\$35/hr	\$10,500
Colasuonno, Chris [Engineer]	300	\$35/hr	\$10,500
Herrmann, Aaron [Engineer]	300	\$35/hr	\$10,500
Caskey, Ryan [Machinist]	30	\$35/hr	\$1,050
Total	930		\$32,550

Chapter 7

Conclusions

In conclusion, overall the system can be considered a success. The objective of the project was to control the position of the ball on the plate for static positions and smooth paths, as well as have the system capable of correcting for disturbances in ball position. In general these goals were accomplished, especially static position balancing and disturbance rejection. The ball can be centered on the plate or another coordinate location, and will quickly correct for even large disturbances to the ball position with fast response time, small overshoot, and a very minimal steady state error. Comparing to the original design specification, the ball is returned to its location with approximately 2% error, however due to touch screen failure, we do not have quantitative data to support this. The settling time is slightly longer than 2 seconds; however in hindsight this may have been extremely fast target for settling a large disturbance. Additionally, the plate is able to track well beyond 1.35 rad/sec. From an observers point of view the system definitely responds well.

As for path following, the more advanced possible objective for this system, there was also a good deal of success. For simple straight line paths, (especially moving along the tilt axis) the system performed moderately well, though there were some slight oscillations about the intended path. It is believed that this could be improved through some improvements to the design of the system.

One apparent issue is related to the system's friction cancellation. With imperfect friction cancellation, there is a possibility that the controller will request a very small torque from the motors but that this request will be less than the remaining friction in the system. Thus, the motor will not actually make this response. This possibility could explain some of the oscillation that occurs during path following. If the friction of the system can more accurately be modelled, perhaps the overall performance of the system could be improved. Lastly, another option would be to recreate the system using nonlinear control methods. This may or may not make an improvement but it would be interesting to examine.

With more time, it would also benefit the system to revise the touch screen interface. The simplicity of using the touch screen controller card and the time limitations of the project lead to the use of the serial communication method. Using the serial connection and touch screen controller card resulted in a limitation of the touch screen resolution of approximately 1024x1024. By devising an interface that uses A/D converters directly on the touch screen output, a much higher resolution could be achieved thus reducing error in the known ball position.

Bibliography

- [1] 3M Touch Systems. *SC3 Touch Screen Controller: User's Guide*, 2nd edition, 2003.
- [2] Dr. Murat Arcaç. Discrete time systems - lecture notes. 2003.
- [3] No Author Available. Control tutorials for matlab: Modeling the ball and beam experiment. Available WWW: <http://wolfman.eos.uoguelph.ca/~jzelek/matlab/ctms/examples/ball/ball1.htm>.
- [4] S. Awtar, C. Bernard, N. Boklund, A. Master, D. Ueda, and K. Craig. Mechatronic design of a ball-on-plate balancing system. Technical report, Rensselaer Polytechnic Institute, 2002.
- [5] Graham Goodwin, Stefan Graebe, and Mario Salgado. Control system design - ball-on-plate tutorial. Available WWW: http://csd.newcastle.edu.au/control/simulations/ball_sim.html, 2001.
- [6] Dr. Russell Kraft. Computer applications lab - hybrid control. 2004.
- [7] Dr. Russell Kraft. Computer applications lab - optimal control. 2004.
- [8] C. Phillips and H. Nagle. Digital control system analysis and design, third edition. Technical report, Prentice Hall, Inc., 1995.
- [9] Eric W. Weisstein. Moment of inertia - sphere. Available WWW: <http://scienceworld.wolfram.com/physics/MomentofInertiaSphere.html>.

Appendix A

Diagrams and Figures

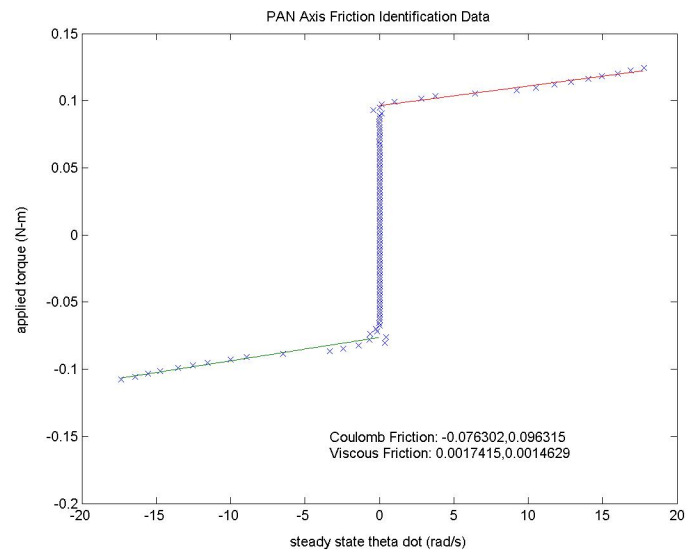


Figure A.1: Pan Axis Friction Data

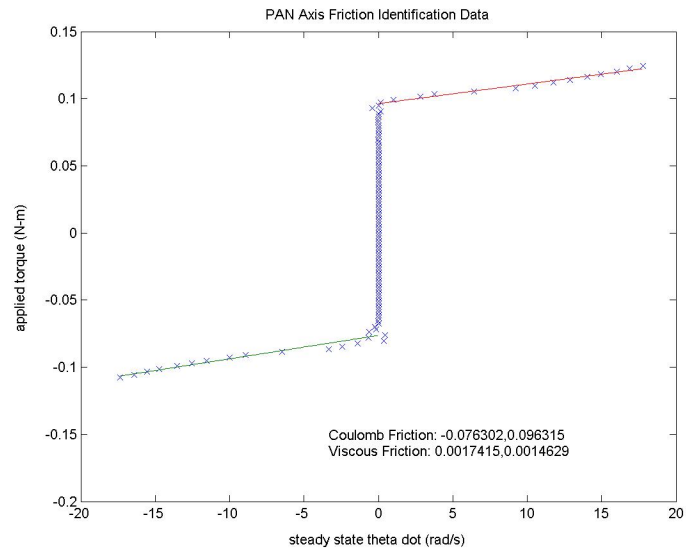


Figure A.2: Tilt Axis Friction Data

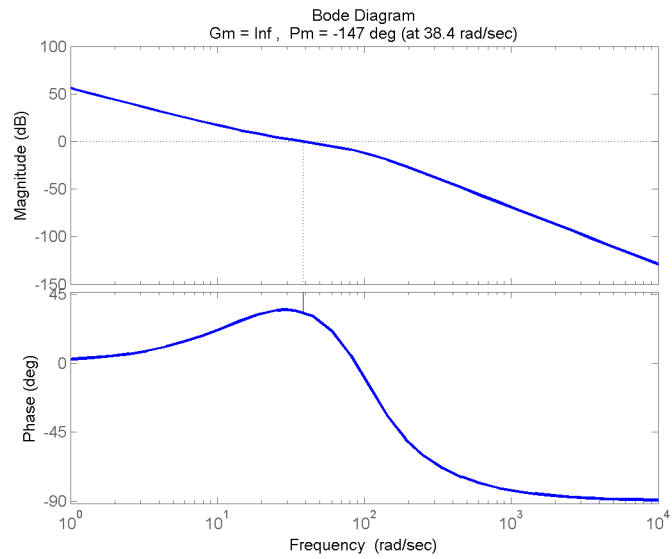


Figure A.3: Frequency Response - Pan Axis

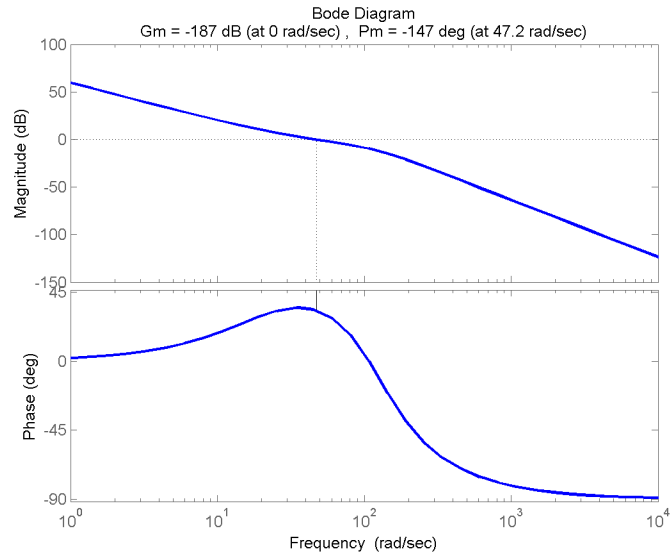


Figure A.4: Frequency Response - Tilt Axis

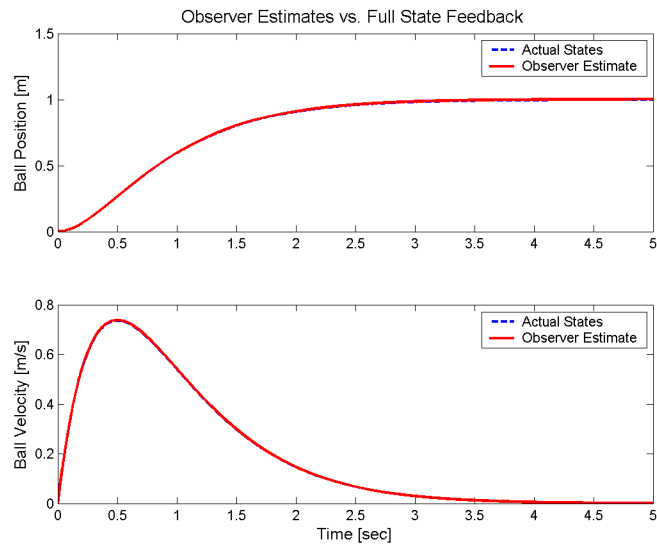


Figure A.5: Observer State Estimation - Ball

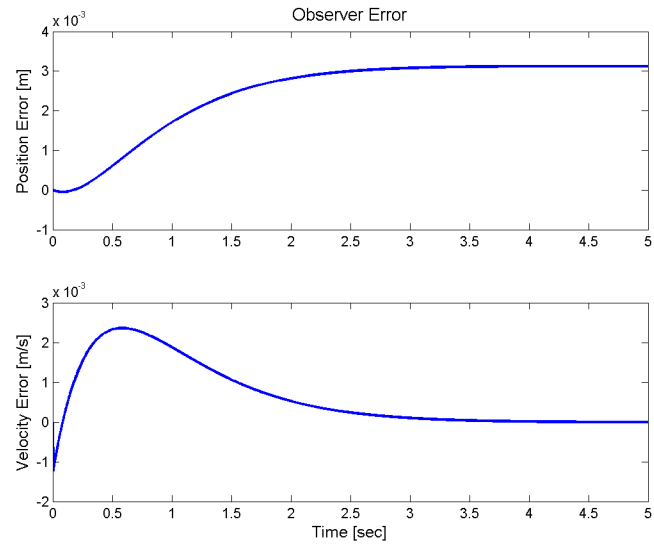


Figure A.6: Observer Error - Ball

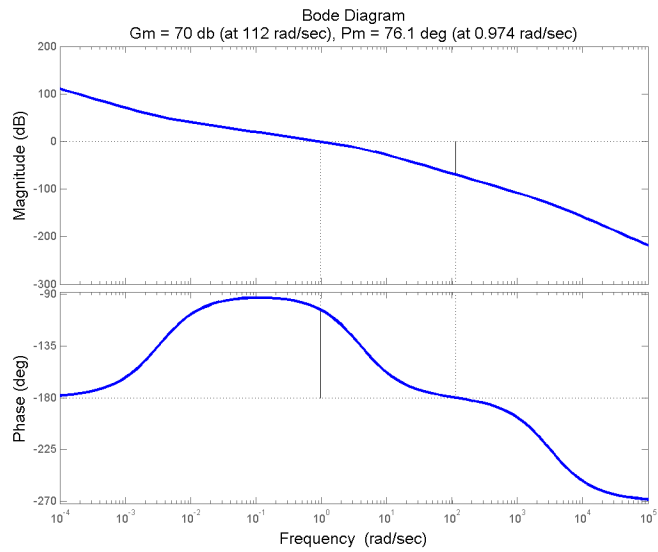


Figure A.7: Frequency Response - Outer-loop

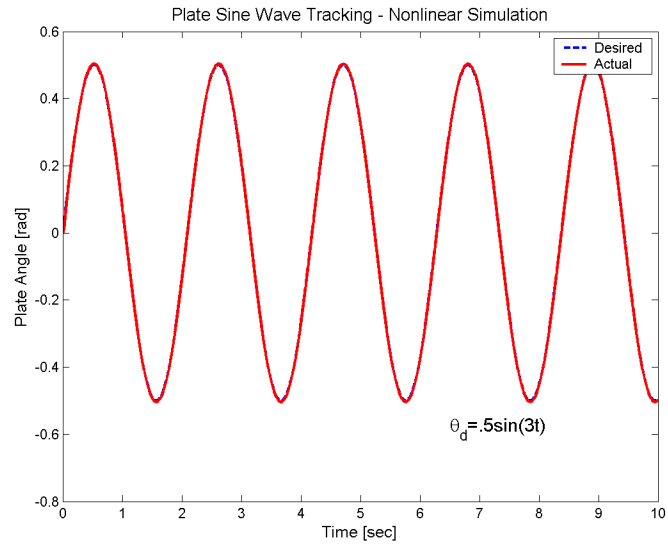


Figure A.8: Plate Sinusoid Tracking - 3 rad/sec

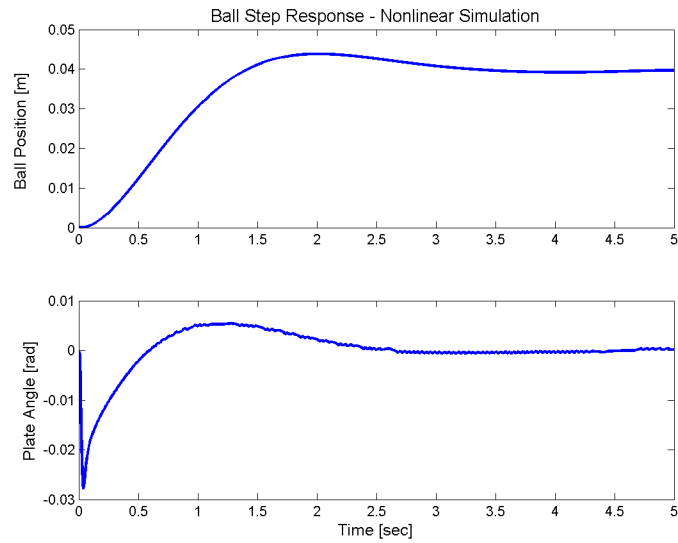


Figure A.9: Ball Position Step Response

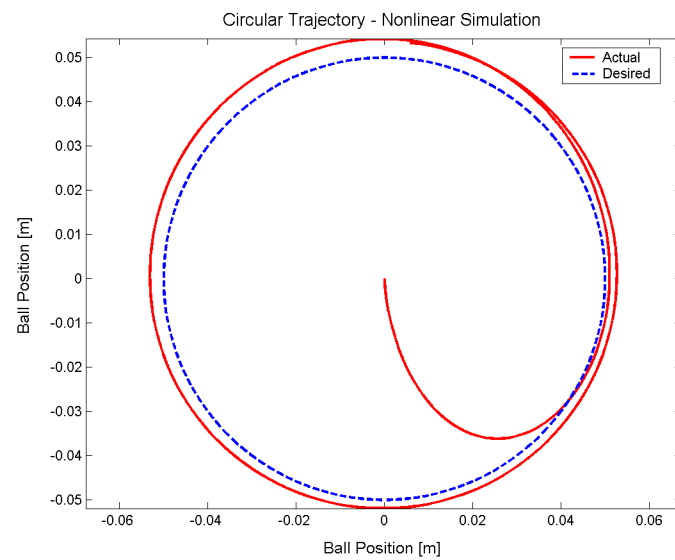


Figure A.10: Ball Circular Trajectory

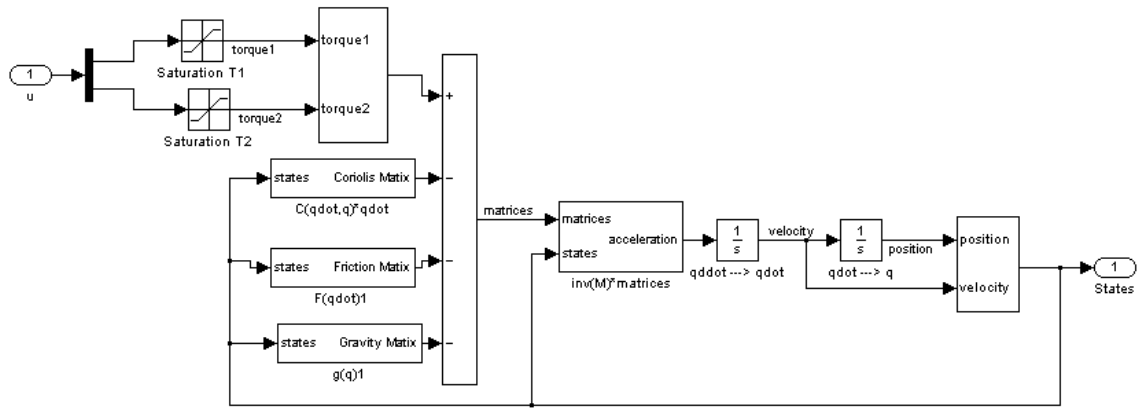


Figure A.11: Nonlinear plate dynamics block diagram

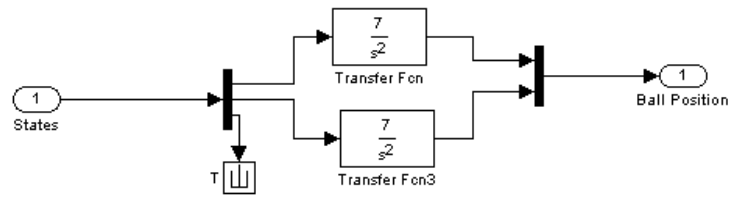
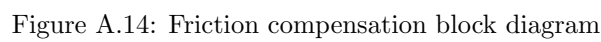


Figure A.12: Linear ball dynamics block diagram



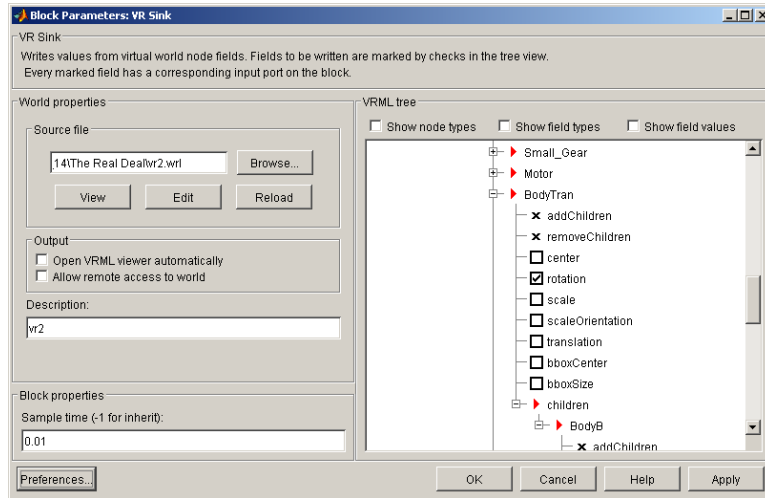


Figure A.15: VR Sink Parameters Window

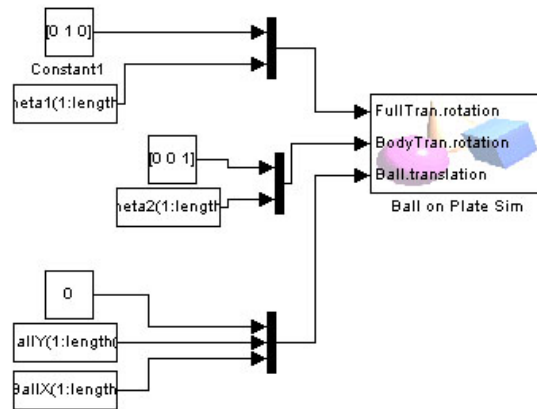


Figure A.16: Virtual Reality Simulation Block Diagram

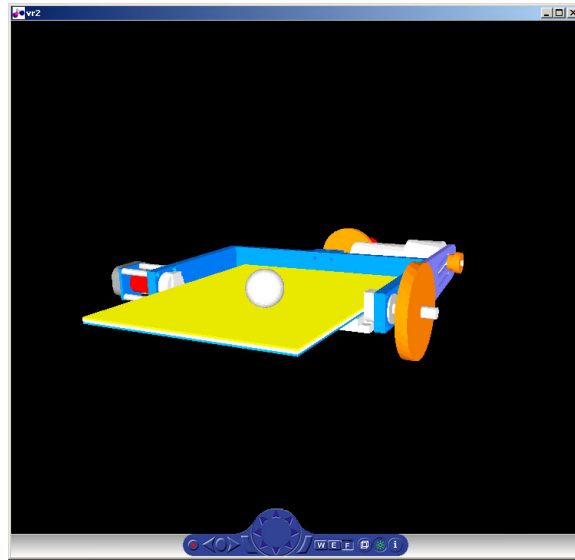


Figure A.17: Virtual Reality Animation Window

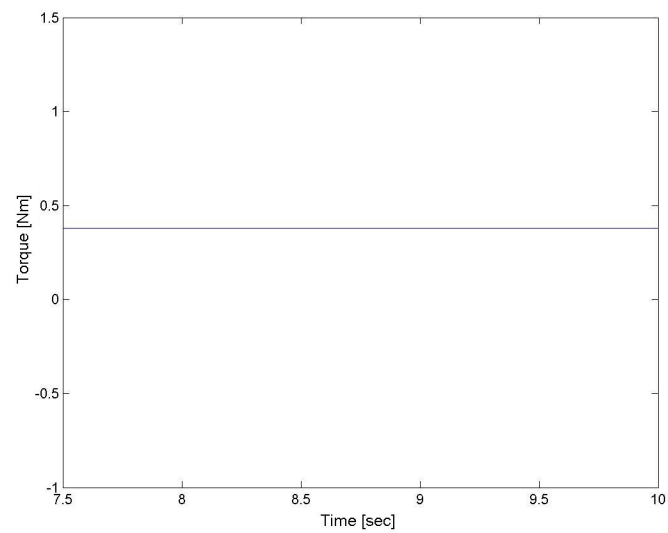


Figure A.18: Gravity cancellation

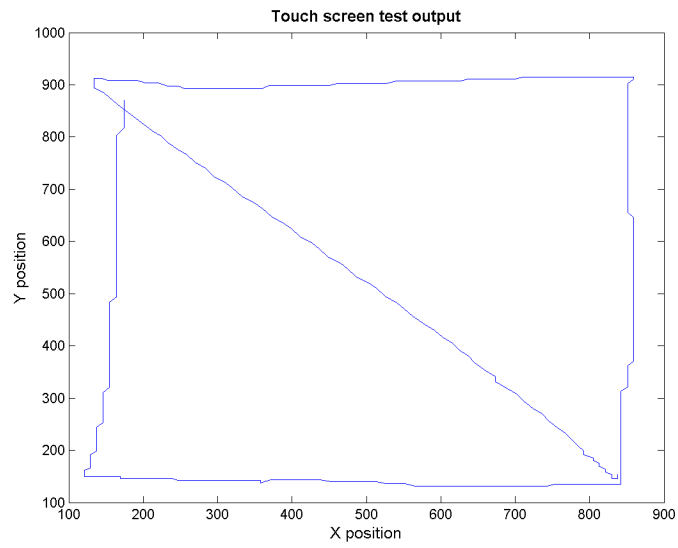


Figure A.19: Touch screen output test (Simple)

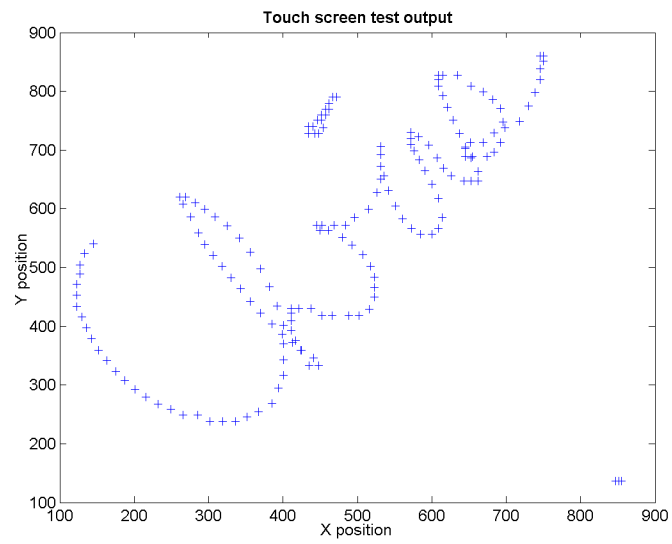
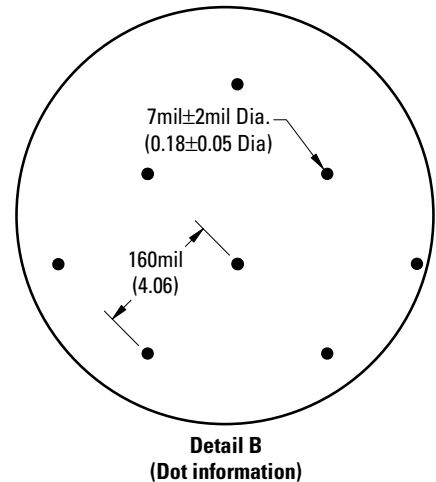
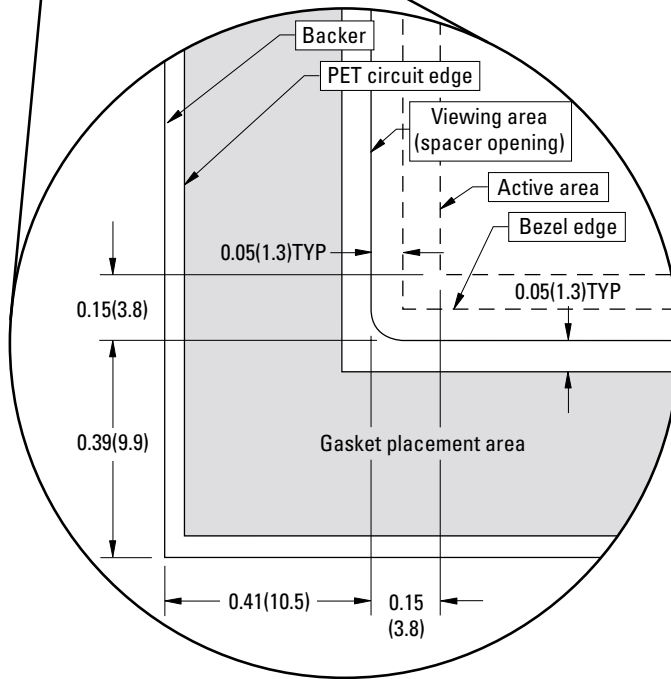
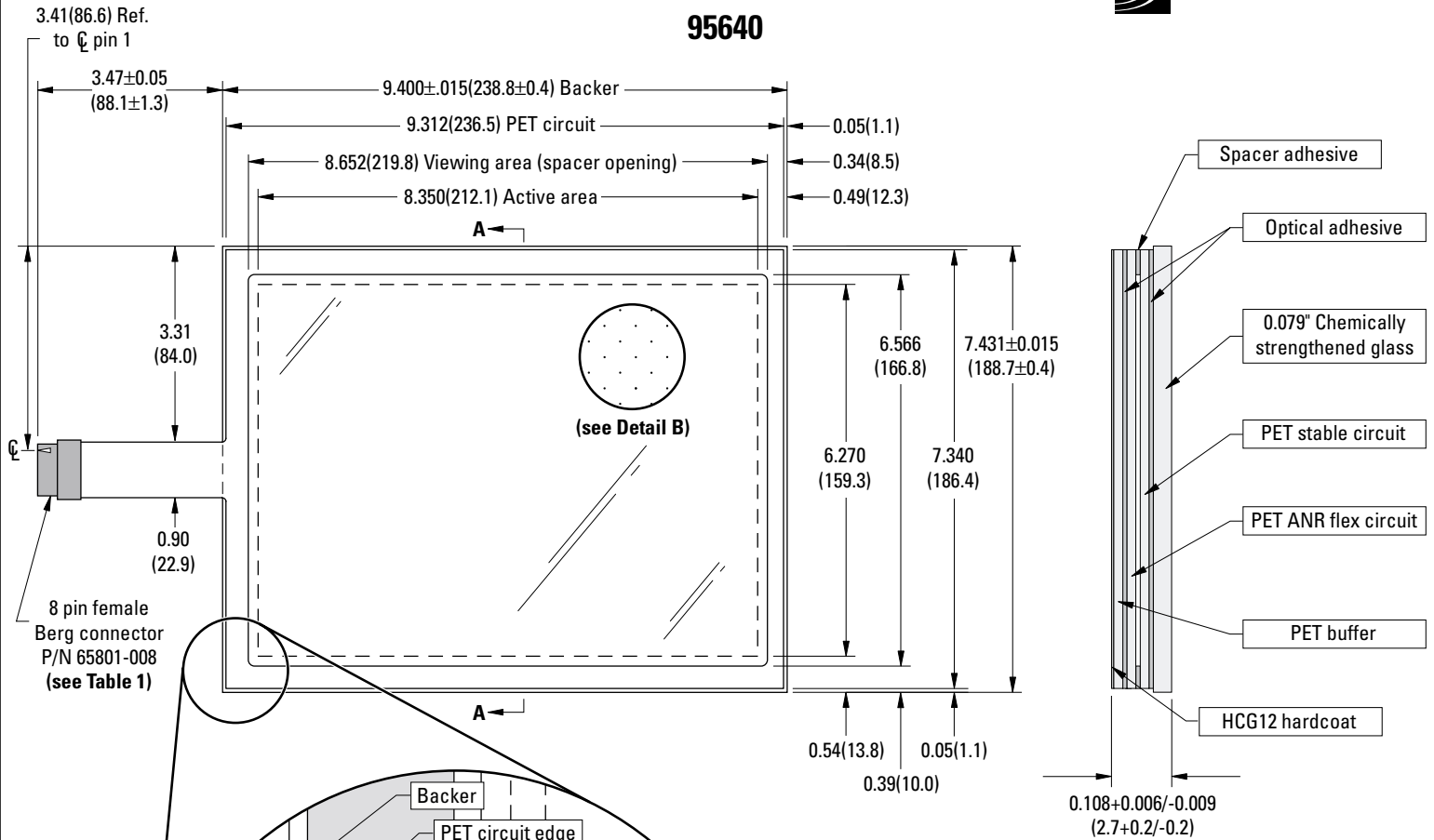


Figure A.20: Touch screen output test (Complex)

Appendix B

Datasheets

10.4" Resistive Touch Screen 95640



Pin#	Assignment
1	Right excite
2	Right sense
3	Left sense
4	Left excite
5	Top excite
6	Top sense
7	Bottom sense
8	Bottom excite

Table 1
(pin assignments)

Tolerances

All tolerances unless otherwise stated, as follows:

Decimal tolerance

(1.)	\pm .05
(1.0)	\pm .05
(1.00)	\pm .03
(1.000)	\pm .010

All dimensions in inches (mm for reference only)
Not to scale

Notes

- Workmanship standard per DTF document PS014, rev. current
- Recognized to U.S. and Canadian requirements under the Component Recognition Program of Underwriters Laboratories Inc.
- Refer to:
 - Dynapro Touch Screen Integration Guide.
 - Data sheet 1005 for hardcoat specifications.
 - Data sheet 1001 for full PL type specifications.
 - Stock touch screen drawing no. 95640-34 rev. current.

Call Toll-Free 1-888-222-9214
www.dynapro.com

GM9234S017

Lo-Cog® DC Gearmotor



Assembly Data	Symbol	Units	Value
Reference Voltage	E	V	24
No-Load Speed	S_{NL}	rpm (rad/s)	424 (44.4)
Continuous Torque (Max.) ¹	T_C	oz-in (N-m)	61 (4.3E-01)
Peak Torque (Stall) ²	T_{PK}	oz-in (N-m)	304 (2.1E+00)
Weight	W_M	oz (g)	16.0 (454)
Motor Data			
Torque Constant	K_T	oz-in/A (N-m/A)	6.50 (4.59E-02)
Back-EMF Constant	K_E	V/krpm (V/rad/s)	4.81 (4.59E-02)
Resistance	R_T	Ω	4.62
Inductance	L	mH	3.97
No-Load Current	I_{NL}	A	0.13
Peak Current (Stall) ²	I_P	A	5.19
Motor Constant	K_M	oz-in/ \sqrt{W} (N-m/ \sqrt{W})	3.01 (2.13E-02)
Friction Torque	T_F	oz-in (N-m)	0.60 (4.2E-03)
Rotor Inertia	J_M	oz-in-s ² (kg-m ²)	5.9E-04 (4.2E-06)
Electrical Time Constant	τ_E	ms	0.85
Mechanical Time Constant	τ_M	ms	9.3
Viscous Damping	D	oz-in/krpm (N-m-s)	0.039 (2.6E-06)
Damping Constant	K_D	oz-in/krpm (N-m-s)	6.7 (4.5E-04)
Maximum Winding Temperature	θ_{MAX}	°F (°C)	311 (155)
Thermal Impedance	R_{TH}	°F/watt (°C/watt)	62.8 (17.1)
Thermal Time Constant	τ_{TH}	min	12.0
Gearbox Data			
Reduction Ratio			11.5
Efficiency ³			0.90
Maximum Allowable Torque		oz-in (N-m)	300 (2.12)
Encoder Data			

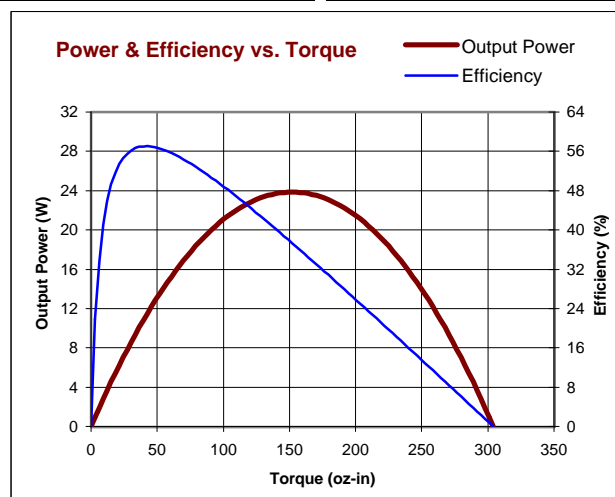
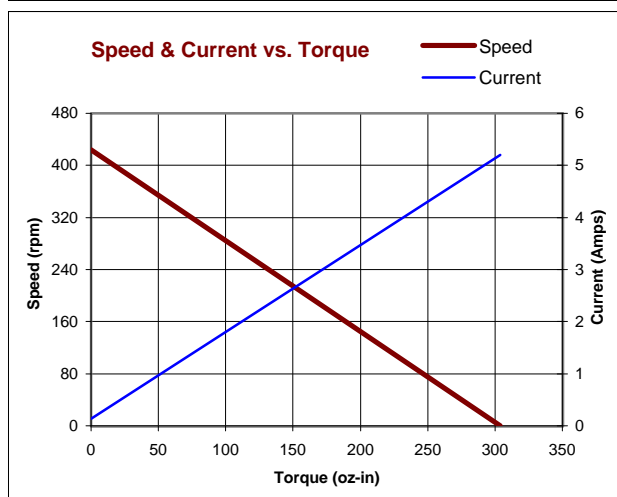
1 - Specified at max. winding temperature at 25°C ambient without heat sink. 2 - Theoretical values supplied for reference only.
3 - Effective gearbox efficiency for this unit improved by use of ball bearings.

Included Features

2-Pole Stator
Ceramic Magnets
Heavy-Gauge Steel Housing
7-Slot Armature
Silicon Steel Laminations
Stainless Steel Shaft
Copper-Graphite Brushes
Diamond Turned Commutator
Motor Ball Bearings
Output Ball Bearing
High Torque Gears

Customization Options

Alternate Winding
Sleeve or Ball Bearings
Modified Output Shaft
Custom Cable Assembly
Special Brushes
EMI/RFI Suppression
Alternate Gear Material
Special Lubricant
Optional Encoder
Fail-Safe Brake



All values are nominal. Specifications subject to change without notice. Graphs are shown for reference only.

© 2001 Pittman.

Appendix C

MATLAB Code

```
% Greg Andrews
% System Linearization and Control System setup
% Control System Design

%Call Simulation Initialization Script
init;

%Symbolic Variables
syms mA mB g t1 t2 lcA1 lcA2 lcA3 lcB1 lcB2 lcB3 Im1 Im2 N1 N2
syms IA11 IA12 IA13 IA21 IA22 IA23 IA31 IA32 IA33 syms IB11 IB12
IB13 IB21 IB22 IB23 IB31 IB32 IB33

%Gravity Vector
G1=
-mA*g*sin(t1)*lcA1-mA*g*cos(t1)*lcA2-mB*g*sin(t1)*cos(t2)*lcB1
-mB*g*cos(t1)*lcB2-mB*g*sin(t1)*sin(t2)*lcB3;
G2= -mB*g*cos(t1)*sin(t2)*lcB1+mB*g*cos(t1)*cos(t2)*lcB3;

%Gradient of the Gravity Vector
partial_G=[diff(G1,'t1') diff(G1,'t2'); diff(G2,'t1')
diff(G2,'t2')];

%Mass-Inertia Matrix
M11=
IA33+mA*lcA1^2+mA*lcA2^2+Im1*N1^2+IB11-IB11*cos(t2)^2+mB*lcB2^2...
+mB*lcB3^2-mB*lcB3^2*cos(t2)^2...
-2*sin(t2)*cos(t2)*IB13+2*sin(t2)*cos(t2)*mB*lcB1*lcB3
+cos(t2)^2*IB33+cos(t2)^2*mB*lcB1^2;
M12=
```

```

-sin(t2)*IB12+sin(t2)*mB*lcB1*lcB2+cos(t2)*IB23-cos(t2)*mB*lcB2*lcB3;
M21=
-sin(t2)*IB12+sin(t2)*mB*lcB1*lcB2+cos(t2)*IB23-cos(t2)*mB*lcB2*lcB3;
M22= IB22+mB*lcB1^2+mB*lcB3^2+Im2*N2^2;

M=[M11 M12; M21 M22];

% Numerical Parameters
g=9.81; Im1=11.5; Im2=11.5;

mA = 0.9690;           % mass of link A in Kg
lcA1 = .0016;          % distance to COM
lcA2 = -.0401; lcA3 = -.1367;

mB = 0.3872; lcB1 = -.0028; lcB2 = -.0406; lcB3 = .0003;

N1=2*11.5;             % total gear ratio
N2=4*11.5;

IA11 = .027716;        % inertia
IA12 = -.000122; IA13 = -.000253; IA21 = -.000122; IA22 = .020929;
IA23 = .006546; IA31 = -.000253; IA32 = .006546; IA33 = .007022;

IB11 = .004464; IB12 = 0; IB13 = -.000001; IB21 = 0; IB22 =
0.001030; IB23 = 0; IB31 = -0.000001; IB32 = 0; IB33 = .003540;

fc1 = .097;            % friction
fv1 = .0019; fv2 = 0.00784; fc2 = 0.00784;

t1=0; t2=0;

G_lin=vpa(subs(partial_G)); M_lin=vpa(subs(M)); Fv=[fv1 0; 0 fv2];

Astuff1=-inv(M_lin)*G_lin; Astuff2=-inv(M_lin)*Fv;

% State space representation
A=[0 0 1 0; 0 0 0 1; Astuff1(1,1) Astuff1(1,2) Astuff2(1,1)
Astuff2(1,2); Astuff1(2,1) Astuff1(2,2) Astuff2(2,1)
Astuff2(2,2)]; A=subs(A); B=[0 0; 0 0; 1 0; 0 1]; C=[1 0 0 0; 0 1
0 0]; D=[0 0; 0 0];

% LQR Plate
[F,G,H,J]=linmod('gravity'); w1=1000; w2=1000; w3=1; w4=1; Q=[w1 0
0 0;
0 w2 0 0;

```

```

    0 0 w3 0;
    0 0 0 w4];
R=.5*eye(2); K=lqr(A,G,Q,R);

% Observer Plate
sys=ss(A,G,C,D); Qobs=[100000 0; 0 100000];
[kest,L,P]=kalman(sys,Qobs,.01*eye(2)); Obs=reg(sys,K,L);
Obs_d=c2d(Obs,Ts);

% Ball Control
Ab=[0 0 1 0;0 0 0 1;0 0 0 0; 0 0 0 0]; Bb=[0 0; 0 0; -7 0; 0 -7];
Cb=[1 0 0 0; 0 1 0 0]; Db=zeros(2);

P=[-1.25+1.5*j -1.25-1.5*j -1.25+1.5*j -1.25-1.5*j];
Kb=place(Ab,Bb,P);

% Ball Observer
w1=100000; w2=100000; w3=1; w4=1; Q=[w1 0 0 0;
    0 w2 0 0;
    0 0 w3 0;
    0 0 0 w4];
R=.01*eye(2); Lb=lqr(Ab',Cb',Q,R)';
Obs_b=ss(Ab-Bb*Kb-Lb*Cb,Lb,Kb,Db); Obs_bd=c2d(Obs_b,.001);

% Initialization file for simulation
% Edited by Greg Andrews
% Control System Design

Ts = 0.001;           % Controller sampling time
%Kmtr = 0.01447;      % motor torque constant
Kmtr = 2.32e-2;

torque_sat = 1;

motor1_igr=11.5;           % Motor1 internal gear ratio
motor1_nls = 44.4*motor1_igr; % Motor1 no load speed at rotor in Rad/s
motor1_st = 2.1/motor1_igr; % Motor1 stall torque at rotor in Nm

motor2_igr=11.5;           % Motor2 internal gear ratio
motor2_nls = 44.4*motor2_igr; % Motor2 no load speed at rotor in Rad/s
motor2_st = 2.1/motor2_igr; % Motor2 stall torque at rotor in Nm

theta1_start = 0.0; theta2_start = 0.0; thdot1_start = 0.0;
thdot2_start = 0.0;

x_start = 0.0; y_start = 0.0; xdot_start = 0.0; ydot_start = 0.0;

```

```

% Define gravity constant
g = 9.81; % acceleration due to gravity in m /(s^2)
g_b = 9.81;
% Define Joint 1 Parameters
belt1_gr=2;
Ngear1 = belt1_gr*motor1_igr; % gear ratio
Imj1 = 4.2e-6; % inertia of motor rotor in KG*m^2 as seen by encoder
fv1 = 0.08; % viscous friction for joint in NmS/Rad as seen by encoder%
fc1 = 0.008; % coulomb friction for joint in Nm as seen by encoder
fv1 = .049636; fc1 = .048994;

%Our Friction Numbers
fc1 = .097; fv1 = .0019;

% Define Joint 2 Parameters
belt2_gr=4;
Ngear2 = belt2_gr*motor2_igr; % gear ratio

Imj2 = 4.2e-6; % inertia of motor rotor in KG*m^2 as seen by encoder
fv2 = .04; fc2 = .004;
fv2 = 0.00784; % viscous friction for joint in NmS/Rad as seen by encoder
fc2 = 0.00784;
% coulomb friction for joint in Nm as seen by encoder

% Define Link A parameters
m_A = 0.9690; % mass of link A in Kg
lc_a1 = .0016; lc_a2 = -.0401; lc_a3 = -.1367;
%inertia of link A about CG in Kg*m^2
l_A=0; I11_A = .027716; I12_A = -.000122; I13_A = -.000253; I21_A
= -.000122; I22_A = .020929; I23_A = .006546; I31_A = -.000253;
I32_A = .006546; I33_A = .007022;

% Define Link B parameters
m_B = 0.3872; % mass of link B in Kg
lc_b1 = -.0028; lc_b2 = -.0406; lc_b3 = .0003;

% inertia of link B about CG in Kg*m^2
I11_B = .004464; I12_B = 0; I13_B = -.000001; I21_B = 0; I22_B =
0.001030; I23_B = 0; I31_B = -0.000001; I32_B = 0; I33_B =
.003540;

%Define Ball (Link C) Parameters
m_c = .13; r_b = 0.015875; I_B = (2/5)*m_c*(r_b)^2;

```



```

%%-----
%%                                MASS INERTIA MATRIX
%M11 = I33_A + m_A*lc_a1 + m_A*lc_a2 + Imj1*Ngear1 + I22_B*cos(u[2])
%+ m_B*lc_b2 + m_B*lc_b3
%- m_B*((lc_b3)^2)*(cos(u[2]))^2-2*sin(u[2])*cos(u[2])*I13_B
%+ 2*sin(u[2])*cos(u[2])*m_B*lc_b1*lc_b3
%+(cos(u[2]))^2*I33_B + (cos(u[2]))^2*m_B*(lc_b1)^2;
%
%M12 = -sin(u[2])*I12_B+sin(u[2])*m_B*lc_b1*lc_b2+cos(u[2])*I23_B
%-cos(u[2])*m_B*lc_b2*lc_b3
%
%M21 = M12
%
%M22 = (I22_B)^2 + m_B*(lc_b1)^2 + m_B*(lc_b3)^2 + Imj2*Ngear2;
%%-----

%%-----
%%                                CORIOLIS MATRIX
%C11 = 0;
%
%C12 = 2*u[3]*I11_B*cos(u[2])*sin(u[2])+2*u[3]*m_B*(lc_b3)^2*cos(u[2])*sin(u[2])
%-4*u[3]*(cos(u[2]))^2*I13_B+2*u[3]*I13_B
%+ 4*u[3]*(cos(u[2]))^2*m_B*lc_b1*lc_b3- 2*u[3]*m_B*lc_b1*lc_b3
%- 2*u[3]*cos(u[2])*I33_B*sin(u[2])
%- 2*u[3]*cos(u[2])*m_B*(lc_b1)^2*sin(u[2]) - u[3]*cos(u[2])*I12_B
%+ u[4]*cos(u[2])*m_B*lc_b1*lc_b2
%- u[4]*sin(u[2])*I23_B + u[4]*sin(u[2])*m_B*lc_b2*lc_b3
%
%C21 = -u[3]*I11_B*cos(u[2])*sin(u[2]) - u[3]*m_B*(lc_b3)^2*cos(u[2])*sin(u[2])
%$+ 2*u[3]*(cos(u[2]))^2*I13_B - u[3]*I12_B
%-2*u[3]*(cos(u[2]))^2*m_B*lc_b1*lc_b3+ u[3]*m_B*lc_b1*lc_b3 +
%u[3]*cos(u[2])*I33_B*sin(u[2])
%+ u[3]*cos(u[2])*m_B*(lc_b1)^2*sin(u[2]) + (1/2)*u[4]*cos(u[2])*I12_B
%- (1/2)*u[4]*cos(u[2])*m_B*lc_b1*lc_b2
%+ (1/2)*u[4]*sin(u[2])*I23_B - (1/2)*u[4]*sin(u[2])*m_B*lc_b2*lc_b3
%
%C22 = (-1/2)*u[3]*cos(u[2]) + (1/2)*u[3]*cos(u[2])*m_B*lc_b1*lc_b2
%- (1/2)*u[3]*sin(u[2])*I23_B+ (1/2)*u[3]*sin(u[2])*m_B*lc_b2*lc_b3
%%-----

%%-----
%%                                GRAVITY VECTOR
%
```

```

%G1 = -m_A*g*sin(u[1])*lc_a1 - m_A*g*cos(u[1])*lc_a2 - m_B*g*sin(u[1])*cos(u[2])*lc_b1
%- m_B*g*cos(u[1])*lc_b2
%- m_B*g*sin(u[1])*sin(u[2])*lc_b3;
%
%G2 = -m_B*g*cos(u[1])*sin(u[2])*lc_b1 + m_B*g*cos(u[1])*cos(u[2])*lc_b3;

```

Appendix D

CAD Drawings

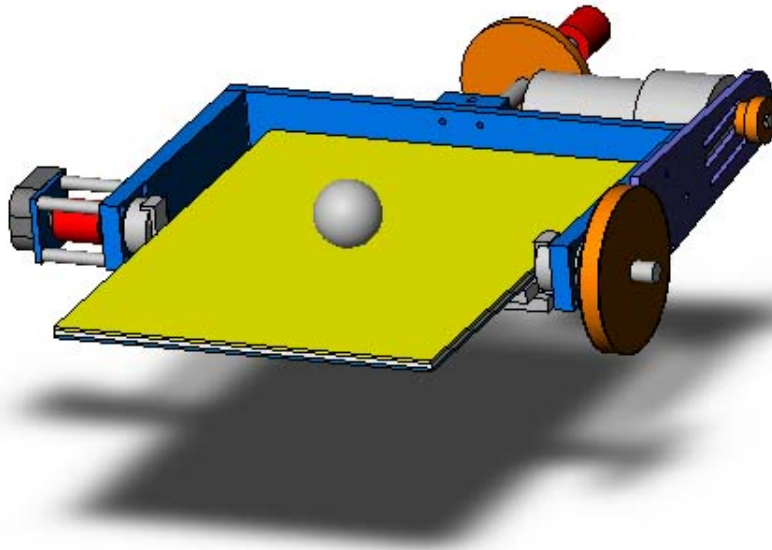


Figure D.1: Full System

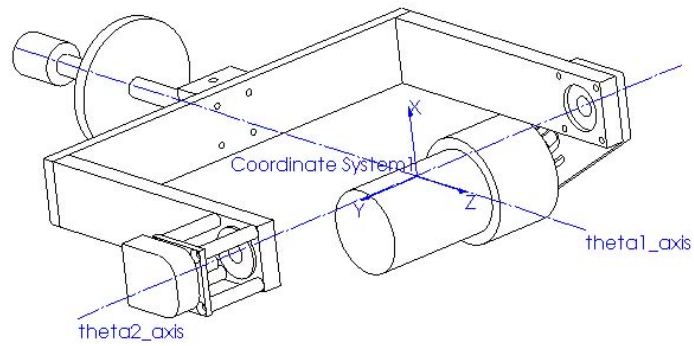


Figure D.2: Body A Coordinate Definitions

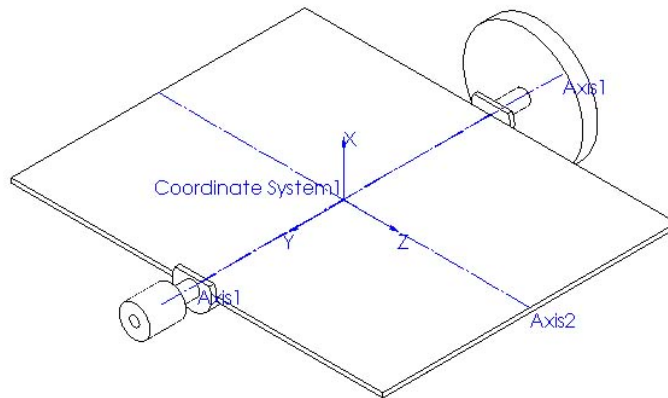


Figure D.3: Body B Coordinate Definitions

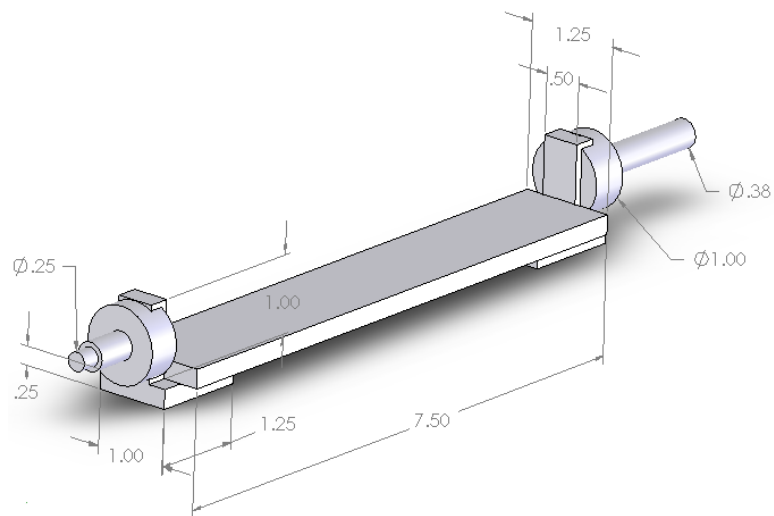


Figure D.4: Axle

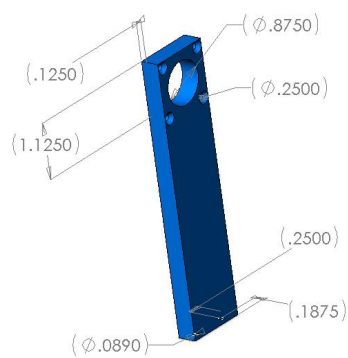


Figure D.5: Encoder Side Bracket

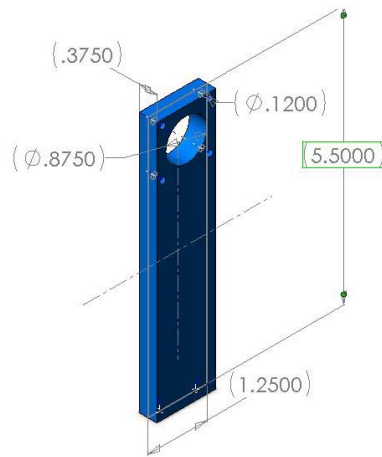


Figure D.6: Motor Side Bracket

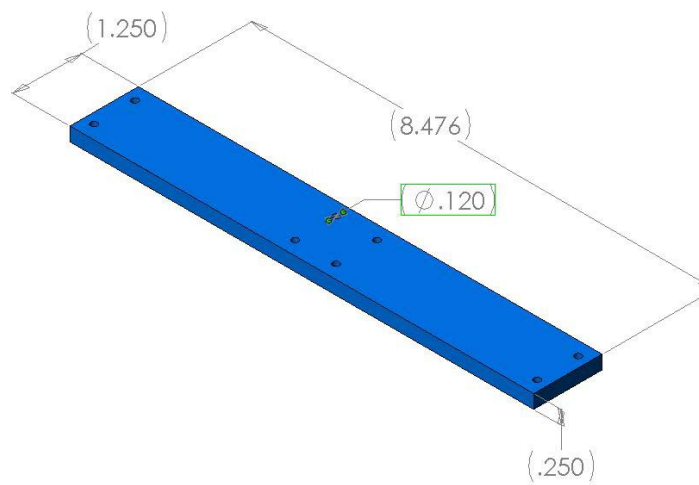


Figure D.7: Yoke Base

Appendix E

Team contributions

Greg completed the following sections:

- Model development
- Control development
- Modelling
- Control
- Simulation

Chris completed the following sections:

- Physical design
- Design Verification
- Conclusions

Aaron completed the following sections:

- Introduction
- Professional & Societal Considerations
- Touch screen subsystem development
- Touch screen subsystem



Greg Andrews



Chris Colasuonno



Aaron Herrmann

Appendix F

Team resumes

83 Squannacook Rd.
Shirley, MA 01464

Home: (978) 448-2783
School: (978) 302-3742
andreg@rpi.edu

Gregory L. Andrews

Objective

To obtain a challenging and rewarding position in the field of Electrical or Computer Engineering

Education

2000-Present Rensselaer Polytechnic Institute Troy, NY

Dual Major in Electrical and Computer & Systems Engineering

- Senior, Concentrating in Automated Control Systems
- *Relevant Coursework:* Control System Design, Voice and Image Processing, Computer Applications Lab, Discrete Time Systems, Fundamentals of Robotics, Signals & Systems, Fields & Waves, Electric Circuits, Data Structures & Algorithms, Differential Equations, Embedded Control

Experience

Winter/Summer 2003 Charles Stark Draper Laboratory Cambridge, MA
Intern

- Helped to develop an optimal control gain scheduling algorithm for an autonomous helicopter, and simulate the system using MATLAB and Simulink.
- Investigated navigation strategies of insects for use in a DARPA supported micro-scale cognitive arthropod project
- Used MATLAB to simulate micro-robotic insects in an indoor environment and create trade-curves relating mission requirements to current technology limitations
- Used MATLAB and C++ to analyze signal attenuation for an under-canopy UAV

Fall 2002 Rensselaer Polytechnic Institute Troy, NY
Introduction to Engineering Design

- Learned principles of the design process while creating a ball testing machine
- Researched and implemented ultrasonic sensors for use in projectile tracking

Fall 2001 Rensselaer Polytechnic Institute Troy, NY
Laboratory Introduction to Embedded Control

- Learned principles of Embedded Control and Hardware/Software interfacing
- Created "Smart Car" using Motorola 68HC11 and C programming language

Summers 1999-2002 Yantra Corporation Tewksbury, MA
Network Administrator

- Administered Network in a Microsoft Windows Domain Environment
- Gained knowledge of networking principles, TCP/IP
- Provided support for company computers, including set-up and repair

Computer Skills

- *Programming:* C / C++ / Java / Perl
- *Operating Systems:* Windows 9x/ME/2000/XP, Linux, Unix
- *Other:* MATLAB, Simulink, Solidworks, LogicWorks, PSpice, Maple, Visual Studio

Campus Address Home Address
1501 Sage Ave. 2240 Scotch Hill Road
Troy, NY 12180 Bloomville, NY 13739

Home phone: (607)-746-7669
Campus phone: (518)-270-1987
Cell phone: (607)-437-7241
E-mail: COLASC@RPI.EDU

Christopher Colasuonno

Objective

To gain experience in engineering through summer employment / internship in a interesting and challenging work environment.

Education

Rensselaer Polytechnic Institute Troy, NY
• B.S. in Computer and Systems Engineering Expected May 2004
and Electrical Engineering
Maintaining a 3.74/4.0 GPA

Engineering Projects

Fundamentals of Robotics, Industrial Robot Lab Fall 2003
• Worked in a team of three to program Staubli and Adept robots for tool assembly and multiple object manipulation tasks.

Software Design and Doc, Peer-to-Peer File Sharing Client Fall 2003
• Worked in a team of two to create a Peer-to-Peer File Sharing Client
• Made use of Universal Modeling Language and Object Oriented Programming Design Patterns

Introduction to Eng Design, Experiment & Measurement Machine Fall 2002
• Worked in a team of eight to create algorithms for a joint project by the class to create a machine for collecting data on the physical properties of balls for use in toys and games
• Took leadership and organized team into subgroups by needed algorithms
• Worked in cooperation with the Sensors and Controls team on data collection and motor controls

Laboratory Introduction to Embedded Controls, Smart Car Fall 2001
• One of a two person team developing a car to follow a track independently
• Programmed Motorola M68HC11 Microcontroller in C for control of car
• Added enhancements for signal lights and automatic turn and reversal of direction

Skills

- 1 Programming and markup language: C/C++, VisualBasic
(MS Visual Studio 6), Perl, OpenGL, LabVIEW, V++, UML, XML, HTML
- 2 Mathematical Scripting: MATLAB 6.5, Maple 7
- 3 Drafting and Circuit Analysis: Solidworks; pSPICE, Capture, Schematics, Logicworks 4.0, espresso
- 4 Excellent computer aptitude: Windows, Macintosh, Unix experience;
Microsoft Office Pro.XP(Word, Excel, Access, PowerPoint, Outlook);
Adobe Photoshop 7.0, Acrobat 5.1

Leadership

- Rensselaer Society of Engineers JM, Inc., Board of Directors **2003-2004**
- Intrafraternity and Intramural Basketball Team Captain **2000-2004**

AARON R. HERRMANN

28 HURDS HILL ROAD
SOUTHBURY, CT 06488

HOME 203-264-0358
CELL 203-525-6297
EMAIL herrma2@rpi.edu

OBJECTIVE

To obtain a full-time electrical engineering position, working in systems engineering and development, starting in June of 2004.

WORK EXPERIENCE

WINTER 2003	AARON ASSOCIATES OF CT, INC.	478 West Main Street Waterbury, CT 06702 MENTOR: Carmen Corvigno
	Co-developed the Supplementary Control and Data Acquisition (SCADA) human-machine interface (HMI) system for the wastewater treatment plant in Westfield, MA. Reduced normal layout time from 3-4 weeks to ~8 days.	
SUMMER 2002	IBM WEBAHEAD, NEXT GENERATION INTERNET TECHNOLOGY	150 Kettletown Road Southbury, CT 06488 MANAGER: Konrad Lagarde
	Migrated and redesigned/developed personal website for John R. Patrick, former Vice President of Internet Technology for IBM. The site was moved from a flat HTML design with JavaScript to one incorporating a simplified management system using PHP and MySQL.	
SUMMER 2001	IBM GLOBAL SERVICES, GLOBAL WEB ARCHITECTURE	150 Kettletown Road Southbury, CT 06488 MANAGER: Les Borde
	Assisted with back end security and configuration on AIX servers by verifying software packages, web server SSL certificates, and valid usernames across IBM internal network (~1700 total servers, routers, firewalls, etc)	
1998 -	DOUBLEARON.COM	
	Self-employed work designing and developing websites for local small businesses Computer tutoring and technical support for members of the local community	

EDUCATION

2000 -	RENSSELAER POLYTECHNIC INSTITUTE	TROY, NY
	Senior, dual majoring in Electrical Engineering and Computer Systems Engineering Concentration in Control Systems Engineering 3.30 GPA Graduating May 2004	

PROGRAMMING EXPERIENCE

Proficient in C, C++, PHP, and Perl
Capable in microcontroller assembly and Java
4+ years of web design experience with HTML, CSS, Javascript and PHP

EMBEDDED DESIGN EXPERIENCE

Currently developing an embedded system to provide timing and scoring for an RPI motorsports group, RallyRPI. Finalized system utilizes Microchip PIC® microprocessors and a custom radio frequency identification (RFID) system to obtain timing information from individual competitor vehicles.
Built autonomous "smart car" using Motorola 68HC11 microcontroller and compiled C; car follows a track using infrared photo-detection and steers using proportional-derivative control algorithm and pulse-width modulation

SOFTWARE EXPERIENCE

ENGINEERING: Cadence PSpice AD, National Instruments LabView, Mathworks Matlab
PROGRAMMING: Microsoft Visual C++, Sun Microsystems JDK
DESIGN: Macromedia Dreamweaver / Flash, Adobe Photoshop / ImageReady

LEADERSHIP EXPERIENCE

Leader of seven person electrical engineering team during semester-long engineering design project
One of the founders and leaders of a new student group, RallyRPI, to create a new motorsports team at RPI

INTERESTS

Web design, digital photography, and competitive motorsports